

AEDC-TR-87-23
DOT/FAA/CT-87/31

file ~~DA315~~
DB
81EN



An Empirical Look at Tolerances in Setting Icing Test Conditions with Particular Application to Icing Similitude

C. S. Bartlett
Sverdrup Technology, Inc.



August 1988

Final Report for Period April 1986 – January 1987

Approved for public release; Distribution is unlimited.

This document is available through the National Technical
Information Service, Springfield, Virginia 22161.

ARNOLD ENGINEERING DEVELOPMENT CENTER
ARNOLD AIR FORCE BASE, TENNESSEE
AIR FORCE SYSTEMS COMMAND
UNITED STATES AIR FORCE

NOTICES

When U. S. Government drawings, specifications, or other data are used for any purpose other than a definitely related Government procurement operation, the Government thereby incurs no responsibility nor any obligation whatsoever, and the fact that the Government may have formulated, furnished, or in any way supplied the said drawings, specifications, or other data, is not to be regarded by implication or otherwise, or in any manner licensing the holder or any other person or corporation, or conveying any rights or permission to manufacture, use, or sell any patented invention that may in any way be related thereto.

Qualified users may obtain copies of this report from the Defense Technical Information Center.

References to named commercial products in this report are not to be considered in any sense as an endorsement of the product by the United States Air Force or the Government.

This report has been reviewed by the Office of Public Affairs (PA) and is releasable to the National Technical Information Service (NTIS). At NTIS, it will be available to the general public, including foreign nations.

APPROVAL STATEMENT

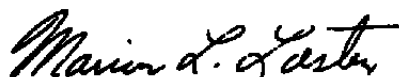
This report has been reviewed and approved.



CARLOS TIRRES
Facility Technology Division
Directorate of Technology
Deputy for Operations

Approved for publication:

FOR THE COMMANDER



MARION L. LASTER
Technical Director
Directorate of Technology
Deputy for Operations

UNCLASSIFIED

SECURITY CLASSIFICATION OF THIS PAGE

REPORT DOCUMENTATION PAGE				Form Approved OMB No. 0704-0188	
1a. REPORT SECURITY CLASSIFICATION UNCLASSIFIED			1b. RESTRICTIVE MARKINGS		
2a. SECURITY CLASSIFICATION AUTHORITY			3. DISTRIBUTION/AVAILABILITY OF REPORT Approved for public release; distribution is unlimited.		
2b. DECLASSIFICATION/DOWNGRADING SCHEDULE			5. MONITORING ORGANIZATION REPORT NUMBER(S) DOT/FAA/CT-87/31		
4. PERFORMING ORGANIZATION REPORT NUMBER(S) AEDC-TR-87-23			7a. NAME OF MONITORING ORGANIZATION		
6a. NAME OF PERFORMING ORGANIZATION Arnold Engineering Development Center		6b. OFFICE SYMBOL (If applicable) DOT		7b. ADDRESS (City, State, and ZIP Code)	
6c. ADDRESS (City, State, and ZIP Code) Air Force Systems Command Arnold Air Force Base, TN 37389-5000			9. PROCUREMENT INSTRUMENT IDENTIFICATION NUMBER		
8a. NAME OF FUNDING/SPONSORING ORGANIZATION Federal Aviation Administration		8b. OFFICE SYMBOL (If applicable)		10. SOURCE OF FUNDING NUMBERS	
8c. ADDRESS (City, State, and ZIP Code) FAA Technical Center, ACT 340 Atlantic City International Airport, NJ 08405			PROGRAM ELEMENT NO. 921H06	PROJECT NO.	TASK NO.
11. TITLE (Include Security Classification) An Empirical Look at Tolerances in Setting Icing Test Conditions with Particular Application to Icing Similitude					
12. PERSONAL AUTHOR(S) Bartlett, C. Scott, Sverdrup Technology, Inc., AEDC Group					
13a. TYPE OF REPORT Final		13b. TIME COVERED FROM 4/86 TO 1/87		14. DATE OF REPORT (Year, Month, Day) August 1988	
15. PAGE COUNT 62					
16. SUPPLEMENTARY NOTATION Frings, Gary, FAA Technical Center Project Manager. Available in Defense Technical Information Center (DTIC) and National Technical Information Service (NTIS).					
17. COSATI CODES			18. SUBJECT TERMS (Continue on reverse if necessary and identify by block number)		
FIELD	GROUP	SUB-GROUP	aircraft icing ice scaling icing tests		
01	02		engine icing ice accretion icing environment		
21	02		icing similitude ice scaling laws		
19. ABSTRACT (Continue on reverse if necessary and identify by block number) An investigation was conducted of the requirements for setting icing test conditions for aircraft engine certification tests. Experimental data were gathered and analyzed to determine how much each of the ice scaling parameters could be allowed to deviate from specified conditions without affecting the similarity of the ice accretions. Also studied were how changes in the ice scaling parameters and changes in the icing test conditions themselves affected the resulting ice shapes. The results indicate that (1) icing similitude criteria must be established in advance of the test; (2) changes in the scaling parameters do not necessarily indicate a change in the ice shape; (3) experimental data are useful in determining allowable changes in the icing test conditions; (4) determination of allowable tolerances for icing test parameters will depend on which icing regime one is operating in; and (5) scaling laws used in this report cannot solely be used to determine tolerances in setting icing test conditions.					
20. DISTRIBUTION/AVAILABILITY OF ABSTRACT <input type="checkbox"/> UNCLASSIFIED/UNLIMITED <input checked="" type="checkbox"/> SAME AS RPT. <input type="checkbox"/> DTIC USERS			21. ABSTRACT SECURITY CLASSIFICATION UNCLASSIFIED		
22a. NAME OF RESPONSIBLE INDIVIDUAL C. L. Garner			22b. TELEPHONE (Include Area Code) (615) 454-7813		22c. OFFICE SYMBOL DOCS

DD Form 1473, JUN 86

Previous editions are obsolete.

SECURITY CLASSIFICATION OF THIS PAGE

UNCLASSIFIED

PREFACE

The work reported herein was conducted by the Arnold Engineering Development Center (AEDC), Air Force Systems Command (AFSC), at the request of the United States Department of Transportation, Federal Aviation Administration (FAA). The analytical study was conducted by Sverdrup Technology, Inc., AEDC Group, operating contractor for the propulsion test facilities at AEDC, AFSC, Arnold Air Force Base, Tennessee, under Project Number DB81EW. The Air Force Project Monitor was Mr. Carlos Tirres, AEDC/DOTR, and the FAA Contracting Officer Technical Representative was Mr. Gary Frings, FAA Technical Center.

CONTENTS

	Page
EXECUTIVE SUMMARY	11
INTRODUCTION	13
Background	13
Objective	13
Scope	13
DISCUSSION	14
Icing Similitude Background with Assumptions	14
Influence of Scaling Parameter Changes on Similitude	16
Influence of Icing Test Condition Changes on Similitude	21
Effect of Temperature	21
Effect of Velocity	22
Effect of Droplet Size	22
Effect of Liquid Water Content	22
Effect of Geometry	22
Effect of Static Pressure	23
Approximate Similitude Trial Results	23
Rime Ice Similitude Test	23
Glaze Ice Similitude Test	24
CONCLUSIONS	24
REFERENCES	26
DISTRIBUTION LIST	54

APPENDIX

A. Facility Description	47
--------------------------------------	-----------

ILLUSTRATIONS

<u>Figure</u>	<u>Page</u>
1. Effect of Air Energy Driving Potential on Ice Shape and Drag; Airfoil, NACA 0012 with 21-in. Chord at 14.7-psia Total Pressure	27
2. Effect of Droplet Energy Driving Potential on Ice Shape Drag; Airfoil, NACA 0012 with 21-in. Chord at 14.7-psia Total Pressure	28
3. Effect of Freezing Fraction on Ice Shape Drag; Airfoil, NACA 0012 with 21-in. Chord at 14.7-psia Total Pressure	29
4. Effect of Accumulation Parameter on Ice Shape Drag; Airfoil, NACA 0012 with 21-in. Chord at 14.7-psia Total Pressure	30
5. Effect of Modified Inertia Parameter on Ice Shape Drag; Airfoil, NACA 0012 with 21-in. Chord at 14.7-psia Total Pressure	31
6. Effect of Static Pressure Changes on Ice Accretions Collected on a 2.0-in.-Diam Cylinder in the AEDC Icing Research Test Cell	32
7. AEDC Icing Research Test Cell Repeatability—Ice Shape Collected on a 2.0-in.-Diam Cylinder	33
8. Effect of Static Air Temperature on Ice Shape Drag with Lines of Constant Calculated Freezing Fraction	34
9. Effect of Total Temperature on Ice Shape; ($LWC \times V \times \text{Time}$) = Constant; MVD, 20 μm ; Airfoil, NACA 0012 with 21-in. Chord at 4-deg Angle of Attack (Ref. 3)	35
10. Effect of Velocity on Ice Shape and Drag; Airfoil, NACA 0012 with 21-in. Chord at 4-deg Angle of Attack (Ref. 3)	36
11. Effect of Droplet Size on Ice Shape and Drag; Airfoil, NACA 0012 with 21-in. Chord at 4-deg Angle of Attack (Ref. 3)	37
A. Drag Change	37
B. Ice Shapes	38

Figure**Page**

12. Effect of LWC on Ice Shape and Drag; Airfoil, NACA 0012 with 21-in. Chord at 4-deg Angle of Attack (Ref. 3)	39
13. Effects of LWC Variations on Laminar Flow Airfoil, 12-in. Chord, 0-deg Angle of Attack, 8-min Cloud Duration (Shown 90-percent Full-Scale)	40
A. Part 1	40
B. Part 2	41
14. Effect of LWC Variations on Different Airfoils at the Same Icing Test Conditions (Ref. 4)	42
15. Airfoil Geometry Details (Ref. 4)	43
16. Approximate Similitude Results for Rime and Glaze Ice Baseline Icing Conditions, Laminar Flow Airfoil, 12-in. Chord, 0-deg Angle of Attack	44
A. Rime Ice	44
B. Glaze Ice	44

TABLES

1. Tabulation of Icing Conditions and Scaling Parameters for Ref. 3 Data Used in This Report	45
2. Scaling Parameters for Approximate Similitude Trials	46

LIST OF ABBREVIATIONS

A	Area, ft ²
A_c	Accumulation parameter, dimensionless
AEDC	Arnold Engineering Development Center
Btu	British thermal unit
c	Characteristic length, diameter for cylinders, and leading edge diameter for airfoils, inches
C_d	Section drag coefficient (as measured in Ref. 3)
c_p	Specific heat at constant pressure, Btu/(lbm-°F)
ETF	Engine Test Facility
F_d	Force caused by section drag, lbf
fps	Feet per second, ft/sec
g_c	Universal gravitational constant, 32.174 (lbm-ft/lbf-sec ²)
h_c	Convective heat-transfer coefficient, Btu/(ft ² -hr-°F)
IRT	Icing Research Tunnel, NASA LeRC
J	Mechanical equivalent of heat, 778 (ft-lbf)/Btu
K	Inertia parameter, dimensionless
K_o	Modified inertia parameter, dimensionless
LWC	Liquid water content, gm/m ³
L_v	Latent heat of vaporization, Btu/lbm
LeRC	Lewis Research Center, NASA

M	Mach number, dimensionless
MVD	Mean volume droplet diameter, μm
N	Stagnation point freezing fraction, dimensionless
P	Pressure, psia
T	Temperature, $^{\circ}\text{F}$
t	Icing time, seconds, minutes
V	Velocity, ft/sec
We	Evaporative mass flux, $\text{lbm}/(\text{ft}\cdot\text{sec})$

GREEK SYMBOLS

α	Angle of attack, degrees
β	Local collection efficiency, dimensionless
θ	Air energy driving potential, $^{\circ}\text{F}$
λ	Droplet range parameter, dimensionless
ρ	Density, lbm/ft^3
ϕ	Droplet energy driving potential, $^{\circ}\text{F}$

SUBSCRIPTS

a	Air
i	Ice
s	Static condition
sur	Surface

t **Total (stagnation) conditions**

w **Liquid water**

∞ **Free-stream condition**

EXECUTIVE SUMMARY

Often, engine icing tests cannot be conducted at conditions that are considered the critical test points because of aircraft engine test facility operational constraints or the inability to find the desired conditions in natural icing flight tests. The use of ice scaling laws may circumvent this testing limitation. Earlier studies (Refs. 1 and 2) of the application of ice scaling (similitude) to aircraft engine testing indicated that experimental data were needed to determine to what extent icing test conditions [temperature (T), velocity (V), liquid water content (LWC), median volume diameter (MVD), pressure (P)], could vary and still achieve similar test results.

In this investigation, experimental data were gathered and analyzed to determine how much each of the ice scaling parameters could vary without affecting similitude.

Also studied were the effects of changing the ice scaling parameters and the icing test conditions on the resulting ice shapes. This effort used ice shape and associated drag coefficient data collected during other studies as well as new ice shape data which was collected as a part of this study.

The results of this study indicate that

1. Icing similitude criteria should be established in advance of the test in order to focus attention on the critical components and critical icing test conditions.
2. Changes in the ice scaling parameters do not necessarily indicate a quantifiable change in the ice shape (similitude).
3. Experimental data are useful in determining allowable changes in the icing test conditions (T, LWC, MVD, V, time) and may be a useful indicator of similitude in some icing regimes.
4. Determination of allowable tolerances for the icing test parameters depend on which icing regime one is operating in (e.g., rime or glaze ice). (Glaze ice accretions are generally less tolerant to changes in test conditions.)
5. The scaling law used herein cannot solely be used to determine tolerances in setting test conditions.

INTRODUCTION

BACKGROUND.

A set of ice scaling laws was analyzed and experimentally verified at the Arnold Engineering Development Center (AEDC) by Ruff (Ref. 1). These same scaling laws were used as the basis for an analytical study addressing the use of the scaling laws to facilitate aircraft engine icing testing (Ref. 2). The particular form of ice scaling (icing similitude) investigated in Ref. 2 was called parameter substitution. The intent of parameter substitution was to generate similar ice shapes under differing meteorological and operational conditions. Similar, in this case, referred to reasonable geometric shape and similar surface characteristics such as type of ice and surface roughness. An assumption was made in both of these works that to achieve similitude, exact solutions to a set of ice scaling equations must be found. To do this, the value of each of five ice scaling parameters must be maintained constant between the original icing condition and the new icing condition. It should be noted that the five scaling parameters had been found to be sufficient to ensure icing similitude, but it was not known if all of them were necessary. The results of the analysis conducted and presented in Ref. 2 indicated that if any one of the icing test conditions [temperature (T), velocity (V), liquid water content (LWC), median volume diameter (MVD), etc.] was allowed to vary, all of the remaining conditions must also be varied to achieve an exact solution to the scaling law equations and thus ensure a similar ice shape (similitude). The requirement of how close these scaling parameters needed to be to the exact values to achieve approximate similarity could not be answered analytically.

For this reason, this study was undertaken to use experimental data to answer the question of how much variation from the exact values of the ice scaling parameters is tolerable while maintaining approximate similitude and, therefore, to conduct icing tests with valid results.

OBJECTIVE.

The objective of this effort was to develop icing parameter substitution criteria and to provide additional insight and understanding of this technology.

SCOPE.

The methodology employed to develop icing parameter substitution criteria was to evaluate ice shapes collected at various icing conditions. The icing conditions data corresponding to these known ice shapes were then input into the AEDC similitude computer code (Ref. 1), and ice scaling parameters were generated. A comparison of each ice shape and its associated scaling parameters was then conducted to determine if approximate similitude had been or could be achieved.

This effort was conducted at the AEDC Engine Test Facility (ETF). Data that had previously been collected at the NASA Lewis Research Center (NASA LeRC) Icing Research Tunnel (IRT) (Ref. 3), the Canadian National Research Council High Speed Wind Tunnel, and the Ohio State University 6- by 22-in. Transonic Airflow Facility (Ref. 4) were also used in this study. Additional ice shapes were generated in the AEDC's icing research test cell under this and previous efforts.

Data collected at NASA LeRC clearly demonstrated the influence of different icing conditions on ice shapes. Form drag data were also included in the NASA LeRC data. This allowed the coefficient of drag (C_d) to be used as an index of similitude throughout this report. Correlations were sought to relate ice shape and C_d changes to values of the ice scaling parameters.

DISCUSSION

ICING SIMILITUDE BACKGROUND WITH ASSUMPTIONS.

In most icing similitude reports, the criteria for successful similitude are rarely discussed. From an engineering standpoint, one need only consider what aspects of icing are important. Depending on the particular set of circumstances, those characteristics of the ice formation that are important help determine more precisely what constitutes similitude. Several factors could be considered important where ice accretions are concerned. These include changes in the lift, drag, pitching moment, and stall characteristics of an airfoil or other surfaces exposed to icing. Also of interest is ice, which accumulates on a surface and may subsequently break away and be ingested by an engine or strike a control surface causing damage. Another factor is the growth of ice that blocks an engine flow passage, possibly leading to engine stall, surge, flameout, or other operational problems. Judgment must be exercised to determine the criteria for successful similitude, and one must recognize that the criteria may be different for different applications.

As reported in Refs. 1 and 2, ice scaling is a test procedure used to form similar ice accretions on two geometrically similar objects under different operational, atmospheric, and meteorological conditions. "Similar" in this case implies not only identical shapes but identical surface characteristics, such as the type of ice and roughness. Icing is an accretion process, meaning that each layer of ice is formed on the previous layer. This implies that if the ice accretion process is started on a clean airfoil with surface characteristics similar to the full-scale airfoil, the ice accretion process will continue similarly and produce scaled ice accretions. This statement is the premise of icing scaling and was applied throughout the development of the ice scaling parameters. To apply an ice scaling procedure, a set of equations that accurately modeled the beginning of the icing process was defined (Ref. 1). Also, parameters that related the atmospheric conditions of liquid water content (LWC), median

volume droplet diameter (MVD), icing time (t), temperature (T), pressure (P), and velocity (V) were identified.

The first and most obvious type of ice scaling is that in which the ice accretions are formed on subscale models. The ability to test subscale geometries allows smaller test facilities to conduct a wider range of icing tests. Since smaller test facilities are usually less expensive to operate than larger ones; testing costs should be reduced. Also, facilities large enough to conduct full-scale tests may not exist.

A second type of icing similitude, and of particular interest for this study, is test parameter scaling often referred to as parameter substitution. It is aimed at increasing the simulation capabilities of test facilities. The ice scaling equations are used to indicate how ground test conditions can be modified to simulate the required icing test conditions and thereby avoid facility limitations. For example, a facility may be limited by the ability to deliver $LWC = 2.0 \text{ gm/m}^3$, but a requirement exists to produce an ice accretion at $LWC = 3.0 \text{ gm/m}^3$. The scaling equations may be applied to determine the test conditions required, at $LWC = 2.0 \text{ gm/m}^3$, to simulate the ice accretion that would occur at $LWC = 3.0 \text{ gm/m}^3$.

Icing parameter substitution scaling may be employed to determine the adjustment that must be made in the icing test conditions when a limitation exists in any one of the atmospheric test variables. As pointed out in Ref. 2, if any icing test condition is varied, all of the remaining conditions must also be varied in a prescribed manner to obtain exact solutions to the five scaling parameters. This allows the attainment of reasonable geometric and surface similitude. Any deviation from the prescribed values of each icing test condition will preclude maintaining the exact solution of the scaling equations and could degrade similitude. How much the similitude is degraded, if at all, is discussed in this report.

As mentioned, it was assumed that if the ice accretion process was started on a subscale clean airfoil with surface characteristics similar to the original airfoil the ice accretion process would continue similarly and produce similar ice accretions. Historically, this had been an accepted approach in icing studies. (The validity of this assumption is currently being addressed by the AEDC and NASA.) The analysis performed to determine the set of scaling parameters followed a stagnation line, clean-surface-model concept. This assumes that if the icing phenomena occurring along the stagnation line of the icing component are considered, then the entire surface exposed to icing will be correctly modeled. Provisions are not made in this scaling code to recalculate the scaling parameters as the ice accretion grows and changes the icing characteristics of the surface.

Some other limitations of the analysis methodology used are as follows:

1. Ice shape and surface characteristics are the only criteria for successful similitude.
2. Neither natural nor induced ice shedding is considered (by vibration, heating, or externally induced aerodynamic loading).
3. Ice-protected components are not considered in this study.
4. The issues of ice hardness or surface roughness are not quantitatively addressed.
5. The icing conditions referred to throughout this report address only supercooled cloud droplets.
6. All icing test conditions refer to conditions as they existed at the icing component in question and not as they existed in the free stream.

Additional discussions of these assumptions and limitations are given in Refs. 1 and 2.

INFLUENCE OF SCALING PARAMETER CHANGES ON SIMILITUDE.

Five scaling parameters were used to investigate how a change in one test condition could be compensated for through use of parameter substitution scaling to achieve successful icing similitude. The five scaling parameters considered were

1. **θ , The Air Energy Driving Potential** — θ is a term describing the heat-transfer potential of the air passing over an icing surface. It is formulated by the convective heat-transfer term plus the product of the rate of evaporative mass flux and the latent heat of vaporization, all ratioed to the convective heat-transfer coefficient.
2. **ϕ , The Water Droplet Energy Driving Potential** — ϕ is a measure of the energy transfer potential of the liquid droplets impinging on an icing surface. It is the total enthalpy of the droplets ratioed to the specific heat of the droplets.
3. **N , The Stagnation Line Freezing Fraction** — N is defined as the amount of impinging liquid water that freezes on impact with the collection surface. When N is zero, none of the impinging liquid will freeze on impact. When N is one, all of the impinging liquid will freeze on impact (rime ice).

4. **K_0 , The Modified Inertia Parameter** — K_0 is a term describing the affinity of an obstruction in a flow path to collect droplets entrained in that flow path. The larger the value of K_0 , the more affinity a body has to collect drops.
5. **A_c , The Accumulation Parameter** — A_c is a water-catch term relating the LWC, V , icing time, and collection efficiency terms to a rate of water catch for a particular collection surface. It is not an ice collection term as no accounting has been made for changes in the collection surface attributable to ice formation.

One result of the work reported in Ref. 2 is that the tolerance that must be assigned to each of the scaling parameters to maintain similitude cannot be determined analytically. The objective of this effort was to obtain data to help determine those tolerances if possible. Three sets of ice shape data were examined, those reported in Refs. 3 and 4, and unpublished data collected under this and previous efforts at the AEDC. The values of the five ice scaling parameters were calculated for these shapes. The data collected at NASA LeRC (Ref. 3) were deemed most useful for this particular study since they were collected by systematically varying only one icing test condition at a time over a wide range of values. This facilitates the study of changes of the scaling parameters and how these changes affect icing similitude. The form drag was measured for the data collected at NASA, and the drag coefficient (C_d) was used as an index of similitude by quantitatively indicating how much the shape or ice surface changed as measured by this aerodynamic parameter. The question of how much C_d can be allowed to change and still maintain similitude cannot be generalized since this would be dictated by the particular application. However, this does not prevent using C_d as a similitude "goodness" indicator or index. To indicate the effect that a change in C_d might have, consider the equation for force caused by drag (F_d) for a bluff body given by $F_d = C_d \rho V^2 A / (2g_c)$. It can be seen that drag force is linearly proportional to and influenced by the drag coefficient.

As an overview to the material that follows, the reader will see that it is difficult to speak of allowable tolerances in any one of the scaling parameters without considering the other scaling parameters. The scaling parameters must be regarded as a complete set which defines a similitude solution. It can be seen that the manner in which change in a scaling parameter affects similitude is related to the test condition change, which causes the scaling parameter to vary. The following discussion is intended to clarify this point.

Figures 1 through 5 show the resulting change in C_d when each of the five scaling parameters is varied through a range of values. The changes in the scaling parameters were caused by various factors. Along any particular curve in these figures, only one test condition is changing. All of the icing durations shown on these figures are for 8 minutes. The effect

that changes in static pressure have on the ice accretion process is shown in Fig. 6. It can be seen that pressure effects over the range indicated were negligible.

The limited amount of data shown in Figs. 1, 2, and 3 is not sufficient to define a good curve fit through the data points. The curves for these figures were drawn as the author interpreted the data. It is felt that the spikes in C_d represent a critical icing point where, potentially, flow separation occurs because of the formation of glaze ice horns. The magnitude and exact location of these spikes are not known and would require further drag measurements for a more precise definition.

In Fig. 1, the value of C_d versus the air energy driving potential, θ , is plotted. The expression for θ is given by

$$\theta = T_{\text{sur}} - T_s - \frac{V_{\infty}^2}{2g_c J c_{p_a}} + \frac{We}{h_c} L_v$$

It was shown in Ref. 2 that the value of θ is almost linearly proportional to temperature. At the colder temperatures (higher values of θ), the ice that forms is basically rime, which tends only to increase the chord and leading edge surface roughness. This type of ice has comparatively little influence on the flow field about the surface and consequently little effect on C_d . As the temperature is increased, the ice becomes more glaze in nature, with its typical horns causing large airflow disturbances, possibly flow separation, and thus, greater changes in C_d . At even warmer temperatures, smaller amounts of ice tend to form at the leading edge, as the surface is quite wet and warmer, and ice shedding is probably occurring at a high rate. These small accumulations cause little flow disturbances and, thus, are associated with smaller values of C_d . This trend continues until the collection surface is free of ice and the C_d approaches that of a wet surface.

A similar trend exists as the velocity increases along the velocity variance line of Fig. 1. At the lower values of V , the ice formation is small and represents little flow disturbance. At higher velocities, the horned ice growth represents a big flow disturbance with flow separation possible, leading to larger values of C_d . The effect of velocity changes on C_d is quite dramatic. The ice shapes depicted in Fig. 1 are intended to allow the reader to judge the relationship of changes in C_d to changes in the ice shapes for these particular data.

The extent to which C_d changes as the value of θ is changed is heavily dependent on which factor caused the value of θ to change. This is principally caused by the fact that θ may or may not be a function of the particular test condition that is changing. This is most noticeable in the curves along which only T is varied compared to the curves along which only the V is varied. As the temperature varied for the $MVD = 20\text{-}\mu\text{m}$ curve, a change in θ from a value

of 30 to 50°F represents almost no change in the value of C_d . Along the velocity variance line, a change in θ from 22 to 25°F represents a six-fold increase in the value of C_d . It can be noted here that the slope of the temperature variance line between $\theta = 30^\circ\text{F}$ and $\theta = 50^\circ\text{F}$ is different depending on the value of MVD (14, 20, or 26 μm).

Figure 2 is a plot of C_d versus changes in the droplet energy driving potential, ϕ . The expression for ϕ is given by

$$\phi = 32 - T_s - \frac{V^2}{2g_c J c_{p_{w,s}}}$$

Similar discussions for Fig. 1 can be applied to Fig. 2. Φ (ϕ) is almost a linear function of T , but is only slightly affected by changes in V . The denominator of the term containing V is large, and consequently, effects are small.

Figure 2 shows that in some instances a small change in ϕ may result in a large change in C_d , whereas under other conditions, a large change in ϕ may cause a small change in C_d . It is apparent that this is attributable to the factor (T or V) that caused the value of ϕ to change. As in Fig. 1, it is interesting to note the influence MVD has on the slope of the temperature variance curves of Fig. 2. The change in C_d for smaller drop sizes is less sensitive than for the larger drop sizes.

Relative to both Figs. 1 and 2, neither θ (for $N < 1$) nor ϕ is affected by changes in LWC, MVD, or t , although these conditions are highly influential in the formation of ice and, thus, affect the value of C_d . If plotted on a C_d versus θ or ϕ graph, the change in LWC, MVD, or t would form vertical lines parallel to the C_d axis at a value of θ or ϕ dictated by the other icing conditions. These vertical lines would indicate that no change in θ or ϕ occurs even though C_d is varying. This reinforces the observation that changes in similitude are dependent upon changes in the specific icing test conditions and are not necessarily dependent upon changes in the scaling parameters.

Figure 3 shows the change in C_d for changes in the calculated value of clean airfoil stagnation line freezing fraction (N). N is defined as the percentage of impinging liquid water that freezes on impact with the collection surface. Similar discussions can be made for Fig. 3 as for Figs. 1 and 2. The curves are similar in shape because of the functional dependency of N on test conditions that affect the change in ice shape and, thus, C_d . Again, it depends on which test conditions cause the value of N to change, thereby determining the influence that N has on the value of C_d .

Figure 4 shows the effect of changes in C_d as the clean airfoil accumulation parameter (A_c) is varied. The equation for A_c is given by

$$A_c = \frac{LWC(V_\infty)\theta t}{\rho_i c}$$

As mentioned for the previous figures and shown here as an example, it can be seen that if a test condition (T in this case) that is not in the calculation of the scaling parameter (A_c in this example) is allowed to vary, then large changes in C_d may result with no change in the scaling parameter. Again, the slope of the curves for velocity and LWC are dependent on the other icing test conditions.

Figure 5 shows C_d versus K_o , the modified droplet inertia parameter. The equation for K_o (Ref. 5) is given by $K_o = (\lambda/\lambda_s) K$, where λ/λ_s is the droplet range parameter, and K is the inertia parameter. Again, to relate a change in K_o to a change in C_d depends on which icing conditions caused K_o to change. It was noted that, for all other test conditions held constant, a change in MVD from 14 to 36 μm at $T_s = 15^\circ\text{F}$ caused the value of C_d to increase significantly, but at $T_s = 25^\circ\text{F}$ the C_d barely varied. Among other things, this shows the importance of correct droplet sizing in conducting ice accretion tests. The ice shapes for MVD's of 14, 20, 26, and 36 μm are shown to aid the reader in relating C_d to icing shape changes.

Figure 6 shows the ice shapes collected at the AEDC on a 2-in.-diam cylinder for various values of static pressure ranging from 8 to 14 psia. These pressure ranges correspond to standard altitude values of approximately 16,000 feet down to 1,000 feet. A tabulation of the calculated value of the ice-free cylindrical surface scaling parameter is included. Figure 7 shows the repeatability of ice shapes in the AEDC icing research test cell. These figures show only slight changes to the ice shape for the pressure levels tested. These data indicate that pressure effects alone, in the ranges tested, do not significantly influence ice shape, although pressure changes have a significant influence on the value of θ . This could imply that θ may not be significant as a scaling parameter in the range of pressures tested. These data were collected over a limited range, and the effects of pressure may be different at other icing conditions. This observation does not apply when pressure changes cause changes in local icing conditions due to pressure effects on engine operation or inlet performance.

The purpose of looking at how changes in each ice scaling parameter affect the ice shape is to help determine how close each scaling parameter must be held to its prescribed value to achieve approximate similitude. As pointed out in Ref. 2, it is difficult to determine that allowable deviation. Review and analysis of experimental data and dedicated icing tunnel test data show that the scaling parameters vary for a variety of reasons. Specifically, they vary because of changes in the icing test conditions (T, LWC, MVD, V, and P). The amount

each scaling parameter varies can be attributed to one or more of these icing conditions varying. Because of this, it does not appear that the ice scaling parameters can be used to determine approximate similitude in all icing regimes (rime, glaze, or mixed).

INFLUENCE OF ICING TEST CONDITION CHANGES ON SIMILITUDE.

The ultimate goal of determining how much each scaling parameter can deviate from its prescribed value is to determine the allowable tolerance to which each icing test condition must be held without affecting similitude. With this in mind, when icing similitude or icing testing is considered, it is felt that a more appropriate approach is to ask how much each of the test conditions may be allowed to vary without affecting the ice shape or other desired characteristics adversely. This is still a complicated question, since the variation that can be allowed in each of the icing test conditions is still dependent upon certain criteria for successful similitude. The criteria include, among others, the icing regime (rime, glaze, or mixed), geometry of the icing object, and how close is close enough!

The following is intended to point out the influence that changes in the actual icing test conditions (T , V , LWC , MVD , P) have on changes in ice shape and/or C_d . How changes in the test conditions affect the collection of ice on different geometries is also presented.

Table 1 lists the icing conditions and scaling parameters for the data presented in Figs. 8 through 12.

Effect of Temperature

In Fig. 8, C_d is plotted versus static air temperature for three different values of MVD . Also shown are lines of constant calculated stagnation line freezing fraction. At the colder temperatures (less than -10°F) and at smaller drop sizes ($MVD = 14$ and $20\ \mu\text{m}$), a temperature variation of $\sim 30^\circ\text{F}$ (from -20 to 10°F) results in minimal change in C_d . However, at warmer temperatures (greater than -15°F), a rise of a few degrees (to -20°F) causes a significant increase in the C_d for the same droplet sizes. For the larger droplet sizes (i.e. $26\ \mu\text{m}$), the change in slope of the curve is greater, indicating that C_d is more sensitive to temperature changes. In this case, C_d varies not only because of temperature, but also because of MVD differences. The freezing fraction lines seem to indicate that C_d is reasonably insensitive to changes in static temperature when the freezing fraction, N , ≤ 0.7 . They also indicate that a critical peak in C_d seems to occur when $N \cong 0.3$. These observations may aid in the determination of critical design conditions for icing tests. These are limited data. Additional data need to be collected to further substantiate these observations and add resolution to the curve.

Effect of Velocity

Figure 9 shows the effect of velocity differences on the ice shapes as temperature is varied. Note that the product ($LWC \times V \times t$) is constant. It is sometimes incorrectly assumed that holding this "mass collection" term constant at different icing conditions results in "equal" ice accumulation. The collection efficiency at different velocities is different for the same MVD of 20 μm . The local clean airfoil stagnation line collection efficiency is calculated to be 0.670 for the 190-ft/sec velocity and equal to 0.720 for the 308-ft/sec velocity points. The $A_c = 0.050/\text{min}$ for the 190-ft/sec velocity points, and $A_c = 0.054/\text{min}$ for the 308-ft/sec velocity points. Holding the ($LWC \times V \times t$) term constant does not ensure similitude, nor does it ensure equal amounts of ice accumulation at different icing conditions.

The effects of pure velocity changes on the ice shapes are seen in Fig. 10. Again, the calculated values of the scaling parameters can be found in Table 1. At the higher velocities, the total amount of intercepted water should be higher because of the increase in the water flux to the airfoil. The large ice horns account for the high values of C_d .

Effect of Droplet Size

The effects of changes in drop size can be seen in Fig. 11A. The ice shapes corresponding to the data in Fig. 11A are shown in Fig. 11B. Again, Table 1 lists the values of the scaling parameters. Note the significant change in ice shape that may result from small changes in the droplet size.

Effect of Liquid Water Content

Figure 12 shows the effect of LWC changes on C_d . Comparing ice shape variation caused by changing LWC against ice shape variations caused by changing MVD (Fig. 11B) indicates that MVD changes are more influential. LWC changes seem to have little influence on ice shape at these particular icing conditions.

Similar LWC variations resulted in greater ice shape changes for data collected at the AEDC (Fig. 13). It is believed that these greater changes were caused primarily by the use of a different airfoil from that which was used in the NASA studies.

Effect of Geometry

Figure 14 shows how changes in icing test conditions (LWC in this case) affect various airfoil geometries (Ref. 4). It can be seen that changes in LWC have relatively little effect on the VR-7 airfoil, but have a relatively large effect on the NACA 0012 airfoil. The airfoil geometries are detailed in Fig. 15.

Effect of Static Pressure

The effect of static pressure changes on ice accretion shape is almost negligible (See Fig. 6). However, it is emphasized that these data were taken over a limited range and are indications of changes caused solely by pressure. The data do not account for operational effects that would occur in engines, control surfaces, or inlet systems as the aircraft climbs to altitude. Care must be used in the interpretation of these data as well as all icing data. Conditions that exist at a particular engine component subject to icing are probably not the same as the free-stream icing conditions. This is particularly true for engine applications where the conditions that exist at a particular engine component are a function of flight speed, engine operation, and atmospheric conditions (Refs. 6 and 7).

These discussions point to the need for continuing efforts to develop and validate icing similitude laws. One approach might be development of a set of nondimensional scaling parameters such as those that might result from a classical Buckingham Pi Theorem dimensional analysis. Such an analysis is necessary to mitigate the requirement to study each icing point and each different component (geometry) in detail as it now seems necessary to do. The scaling laws and the scaling parameters as presented by Ruff in Ref. 1 have been shown through experimental verification at the AEDC to be adequate to ensure icing similitude over a limited range. The scaling parameters as they presently exist are difficult to use for finding allowable deviations in setting test conditions and for approximate similitude work. For rime ice accretions, where it can be assumed that the surface thermodynamics are relatively unimportant, the scaling parameters should, ideally, show that temperature effects are small. Currently, the scaling parameters do not readily point out which of the physical processes occurring are important and which are not. The most troublesome of the present scaling parameters in this area seem to be the energy driving potentials, which are not nondimensional terms.

APPROXIMATE SIMILITUDE TRIAL RESULTS.

Rime Ice Similitude Test

An attempt was made to determine a set of icing test conditions, different from a set of baseline conditions, which would account for a rise in temperature and still maintain similitude (similar ice shape). The ice scaling code described in Ref. 1 was used with a few changes. Normally the code requires an input to model velocity ratio; all of the other icing test conditions are determined by holding all five scaling parameters to exact values. For this exercise, the model velocity was set equal to the baseline velocity, and the model temperature was set to a value for which approximate similitude was desired (i.e. 11°F). The code output then specified the required values of P , LWC , MVD , and t to maintain similitude. The proposed value of static pressure recommended by the code was ignored, based on the results of Fig. 6; however, the predicted values of LWC , MVD , and t were used. A baseline icing tunnel test was conducted at the AEDC for a rime ice condition. (A description of the

AEDC icing research test cell is included as Appendix A.) The baseline temperature was -4°F . Another ice shape was collected with all baseline conditions, except the temperature was raised to 10°F . The difference can be seen in Fig. 16A. Note that the resulting ice shape is not similar to the original. A third ice shape was collected. The icing conditions were set to the values of LWC, MVD, and icing time predicted by the code to offset the temperature rise. The resulting ice shape was found to be quite close to the baseline shape. The scaling parameters for the three icing conditions are listed in Table 2. As is typical of experimental studies, the desired test conditions can not always be set exactly. The values shown in Table 2 are those actually set during the tests. Note that the baseline condition and recomputed similitude condition both had a calculated freezing fraction of 1, indicating that the ice was all rime in nature. Based upon this limited test, approximate similitude appears to be achievable in this rime ice case.

Glaze Ice Similitude Test

Another trial was conducted with the ice accretion well into the glaze region. The same procedure was used as mentioned previously. The predicted MVD to help overcome the temperature change from 23 to 28°F was $13\text{ }\mu\text{m}$. Upon inspection of the ice shape taken with $13\text{ }\mu\text{m}$, it was noticed that the impingement limit of the new ice shape was far different from the baseline shape and very close to the leading edge. This normally indicates that the droplets are too small. Another test was indicated. Since the predicted static pressure was not used, the droplet size did not need to change significantly to maintain a constant collection term (A_c). The ice shape was rerun using the modified test conditions and original droplet size in an effort to maintain similar collection characteristics. This did not improve the simulation. Nothing seemed to negate the effects of temperature rise. Considerable run back was noted for the initial 28°F test point of Fig. 16B. This latter simulation once again points out the difficulties associated with attempting to achieve icing similitude in the glaze ice region.

CONCLUSIONS

A study was conducted to investigate the possibility of achieving approximate icing similitude by comparing ice shapes against their corresponding icing scaling parameters. The results of this investigation indicate that:

1. The criteria for establishing icing similitude should be specified in advance of the simulation. Allowable similitude tolerances should also be specified.
2. A change in a particular icing scaling parameter may or may not indicate a change in ice shape (similitude). The reason for this is the functional dependency of a particular scaling parameter (θ , ϕ , N , A_c , K_o) on the icing test conditions (T , LWC, MVD, V , P) that caused the change in the ice shape.

3. It may be more indicative of similitude to consider changes in ice shape brought about by changes in the test conditions rather than changes of the icing scaling parameters.
4. The allowable tolerance in setting icing test conditions will depend upon the similitude application and the particular icing conditions at which the test is to be conducted (e.g., rime versus glaze ice region).
5. As long as the local icing conditions ensure rime ice accretions on the component under consideration (N is approximately > 0.7), similitude is easier to accomplish.
6. For specific temperatures, the LWC term can be decreased to levels that cause the icing surface thermodynamics to return to the rime ice accretion regime, and thereby allows use of the $(LWC \times V \times t)$ term to achieve approximate similitude.
7. The ice scaling laws of Ref. 1 cannot be used to determine allowable tolerances in setting test conditions.
8. The effects of pressure (altitude) on icing similitude in the range studied herein are negligible and can be ignored in these cases. This does not consider the effects of icing due to pressure changes, internal to an engine, for example, nor does it consider how changes in free-stream altitude pressure may change local icing test conditions and, hence, affect ice shape.
9. Additional work is needed to develop other approaches to ice scaling. The ice scaling code employed in this study may be too restrictive.

REFERENCES

1. Ruff, G. A. "Analysis and Verification of the Icing Scaling Equations, Vol. I." AEDC-TR-85-30, (AD-A167976), November 1985.
2. Bartlett, C. S. "An Analytical Study of Icing Similitude for Aircraft Engine Testing." AEDC-TR-86-26, DOT/FAA/CT-86/35, October 1986.
3. Olsen, W., Shaw, J., and Newton, J. "Ice Shapes and the Resulting Drag Increase for a NACA 0012 Airfoil." NASA-TM-83556, January 1984.
4. Flemming, R. J. and Lednicer, D. A. "High Speed Ice Accretion on Rotorcraft Airfoils." United Technologies Corporation, NASA-CR-3910, August 1985.
5. Langmuir, E. and Blodgett, K. B. "A Mathematical Investigation of Water Droplet Trajectories." General Electric Co., ATI 25 223, February 1946.
6. Willbanks, C. E. and Schulz, R. J. "Analytical Study of Icing Simulation for Turbine Engines in Altitude Test Cells." AEDC-TR-73-144 (AD-770069), November 1973.
7. Pheifer, G. D. and Maier, G. P. "Engineering Summary of Powerplant Technical Data." FFA-RD-77-76, July 1977.

	T_t , °F	T_s , °F	LWC, gm/m ³	MVD, μm	V, fps	Time, min
◇	*	*	1.3	14	190	8
○	*	*	1.3	20	190	8
◆	*	*	1.3	26	190	8
□	18	*	1.3	20	*	8

* Indicates This Parameter Varied

Static Air Temperature
Indicated in Parentheses

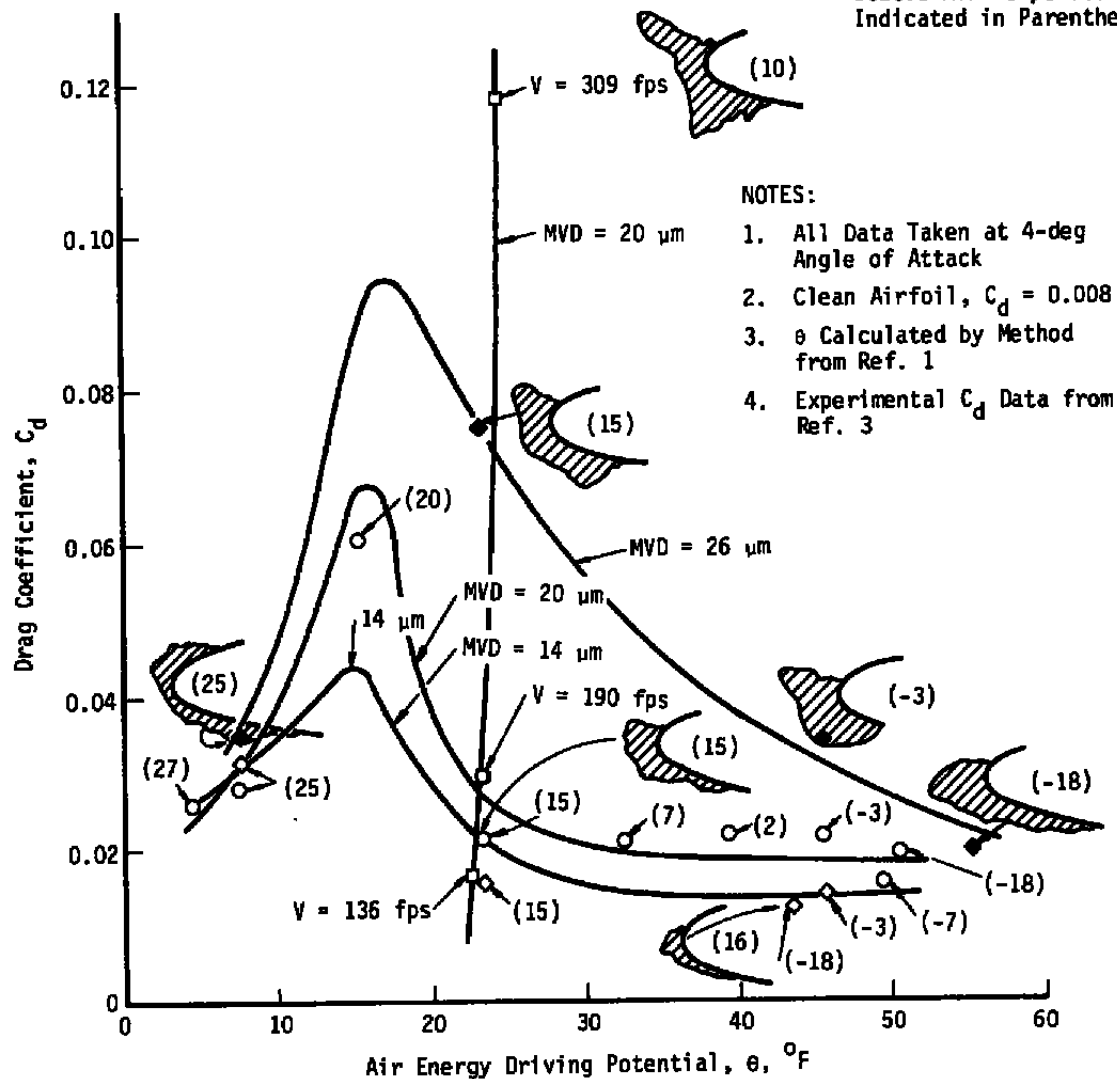


FIGURE 1. EFFECT OF AIR ENERGY DRIVING POTENTIAL ON ICE SHAPE AND DRAG; AIRFOIL, NACA 0012 WITH 21-IN. CHORD AT 14.7-PSIA TOTAL PRESSURE.

	$T_{t, \text{oF}}$	$T_{s, \text{oF}}$	LWC, gm/m^3	MVD, μm	V, fps	Time, min
◇	*	*	1.3	14	190	8
○	*	*	1.3	20	190	8
◆	*	*	1.3	26	190	8
□	18	*	1.3	20	*	8

* Indicates This Parameter Varied

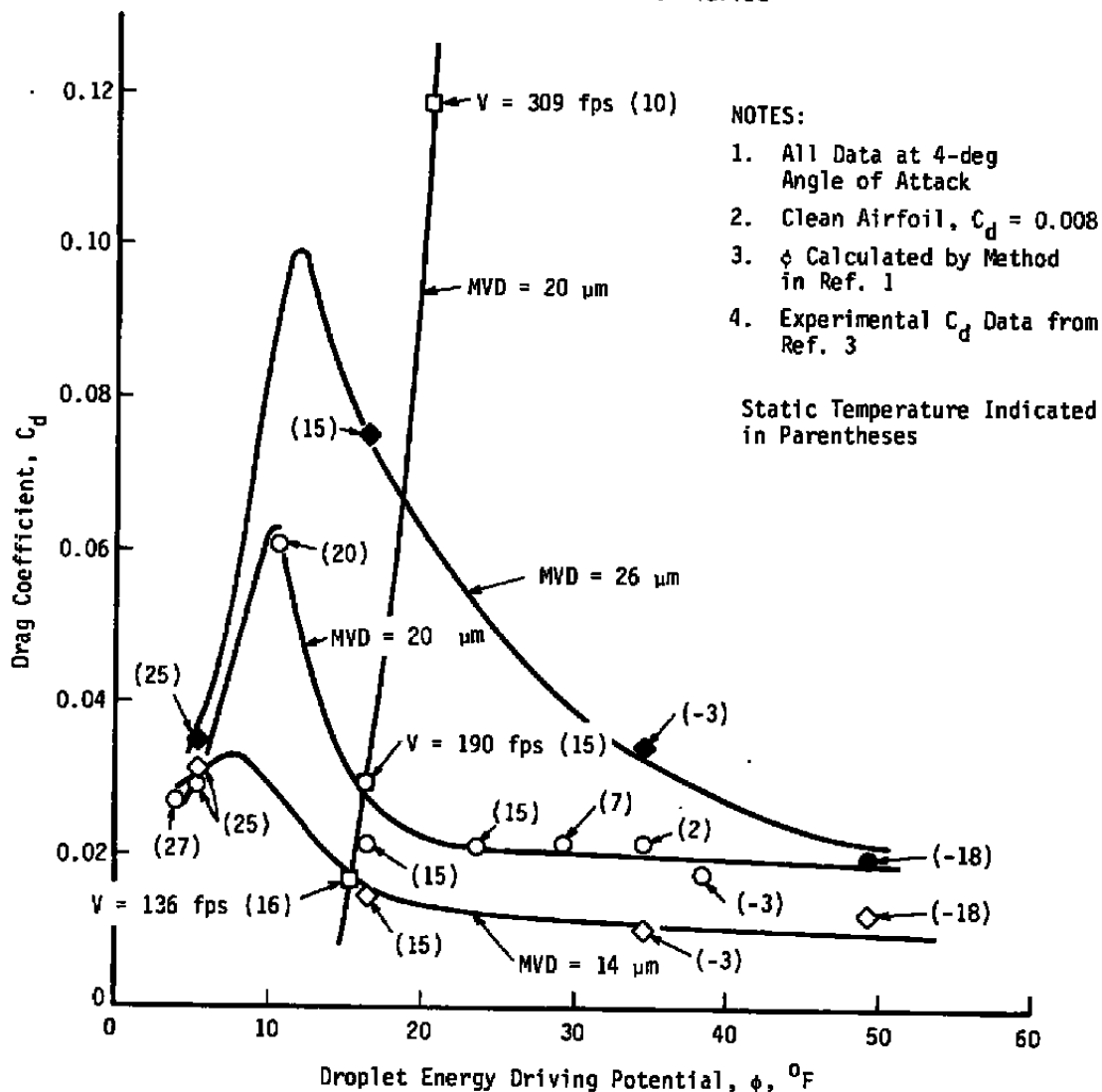


FIGURE 2. EFFECT OF DROPLET ENERGY DRIVING POTENTIAL ON ICE SHAPE DRAG; AIRFOIL, NACA 0012 WITH 21-IN. CHORD AT 14.7-PSIA TOTAL PRESSURE.

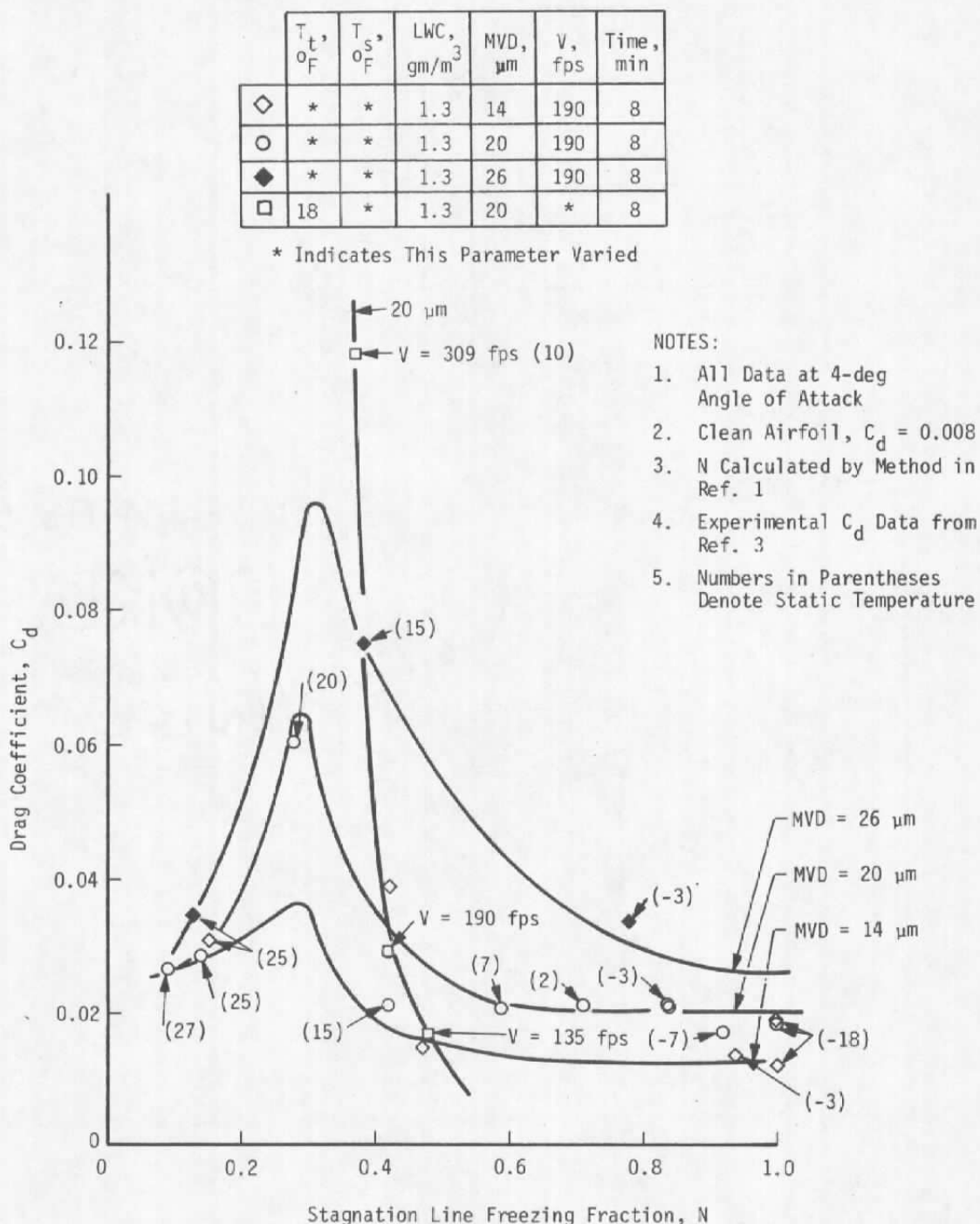


FIGURE 3. EFFECT OF FREEZING FRACTION ON ICE SHAPE DRAG; AIRFOIL, NACA 0012 WITH 21-IN. CHORD AT 14.7-PSIA TOTAL PRESSURE.

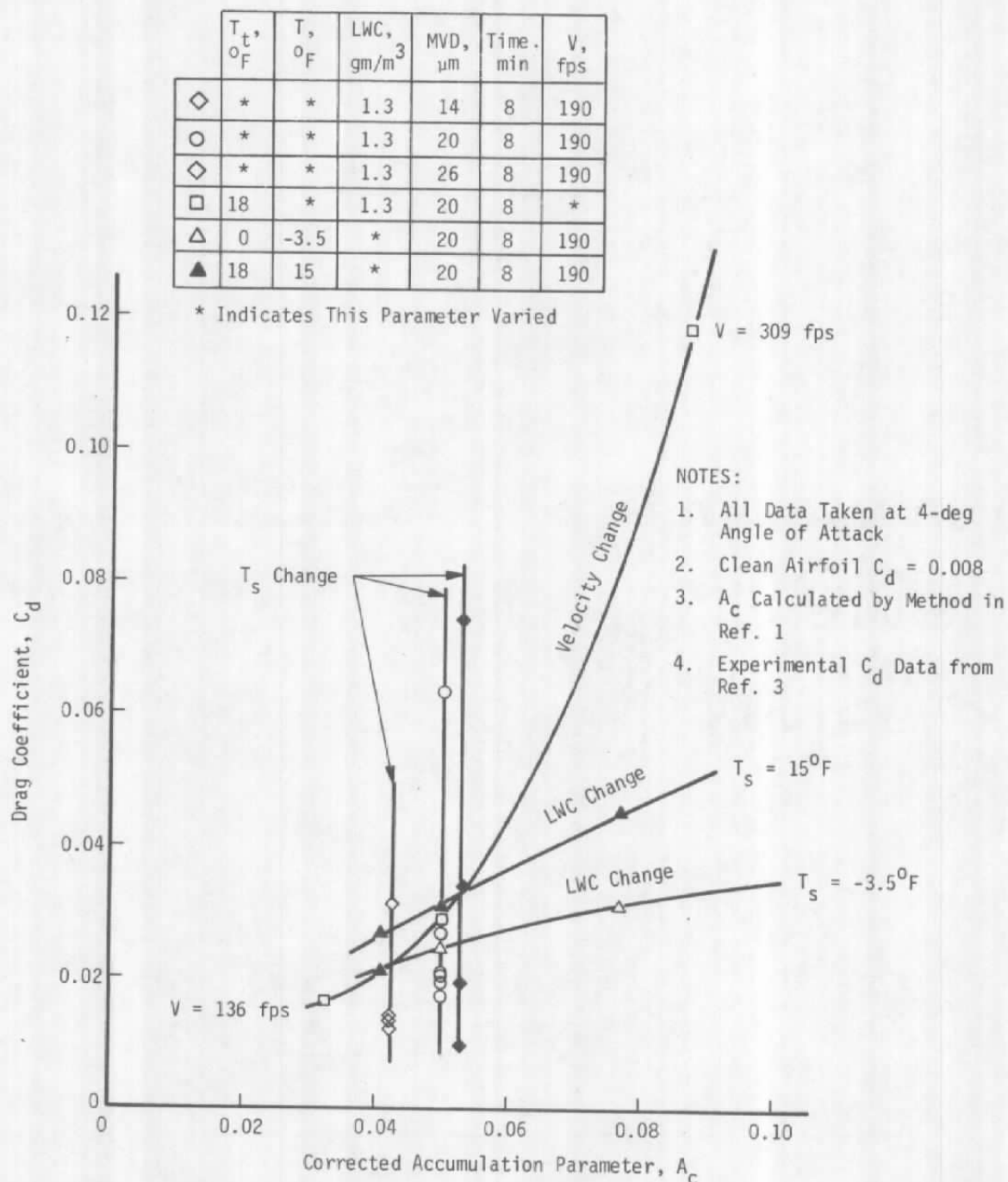


FIGURE 4. EFFECT OF ACCUMULATION PARAMETER ON ICE SHAPE DRAG; AIRFOIL, NACA 0012 WITH 21-IN. CHORD AT 14.7-PSIA TOTAL PRESSURE.

NOTES:

1. Velocity = 190 fps
2. LWC = 1.3 gm/m^3
3. MVD = various
4. Time = 8 min
5. T_s = various
6. T_t = various
7. All Data at 4-deg Angle of Attack
8. Clean Airfoil, $C_d = 0.008$
9. K_0 Calculated by method in Ref. 1
10. Experimental C_d Data from Ref. 3
11. All Ice Shapes Shown for $T = 15^\circ\text{F}$

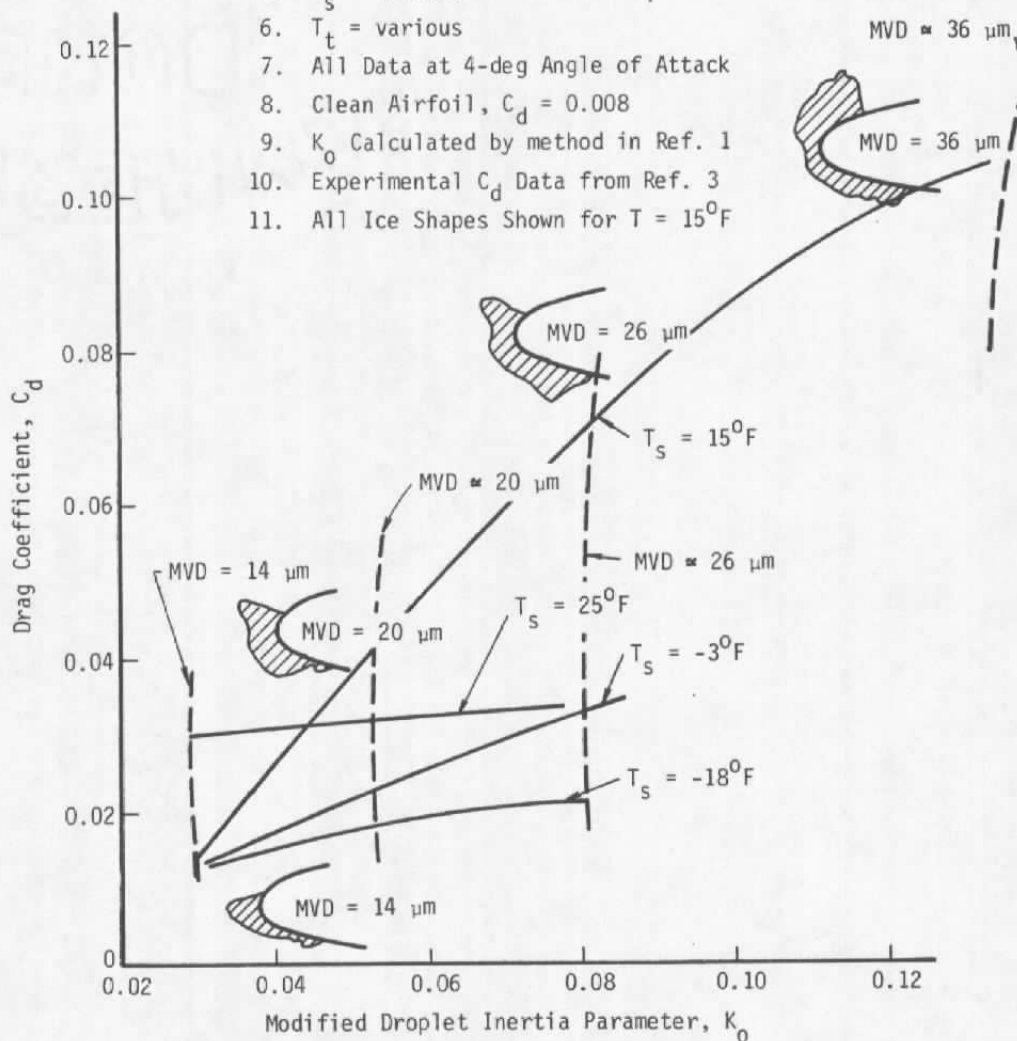
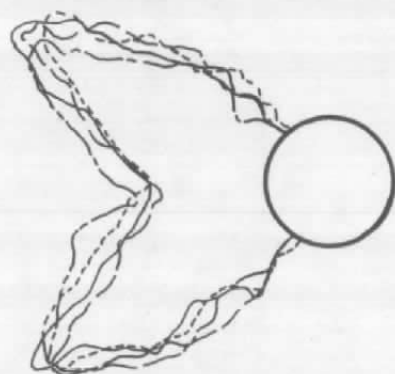
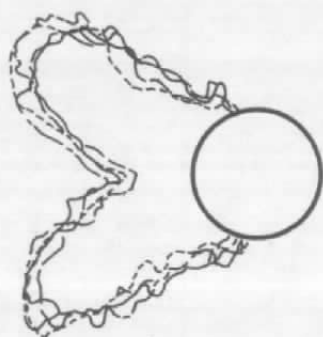


FIGURE 5. EFFECT OF MODIFIED INERTIA PARAMETER ON ICE SHAPE DRAG; AIRFOIL NACA 0012 WITH 21-IN. CHORD AT 14.7-PSIA TOTAL PRESSURE.

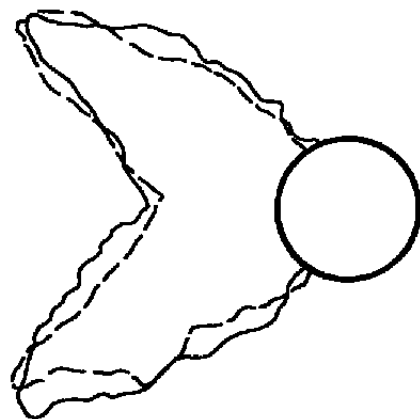


	P, psia	V, fps	T _S , °F	LWC, gm/m ³	MVD, μm	Time, min	θ, °F	φ, °F	N	K _O	A _C
————	14	250	4.0	0.8	28	18	35	27	0.49	2.26	1.43
-----	12	250	4.0	0.8	28	18	37	27	0.48	2.41	1.43
-----	10	250	4.0	0.8	28	18	40	27	0.47	2.59	1.43
- · - · -	8	250	4.0	0.8	28	18	44	27	0.47	2.82	1.43



	P, psia	V, fps	T _S , °F	LWC, gm/m ³	MVD, μm	Time, min	θ, °F	φ, °F	N	K _O	A _C
————	14	250	23	0.8	28	19	9.3	7.0	0.14	2.27	1.43
-----	12	250	23	0.8	28	19	10.0	7.0	0.14	2.41	1.43
-----	10	250	23	0.8	28	19	11.0	7.0	0.14	2.59	1.43
- · - · -	8	250	23	0.8	28	19	13.0	7.0	0.14	2.83	1.43

FIGURE 6. EFFECT OF STATIC PRESSURE CHANGES ON ICE ACCRETIONS COLLECTED ON A 2.0-IN.-DIAM CYLINDER IN THE AEDC ICING RESEARCH TEST CELL.



P, psia	V, fps	T, °F	LWC, gm/m ³	MVD, μm	Time, min
14	250	4.0	0.8	28	18

**FIGURE 7. AEDC ICING RESEARCH TEST CELL REPEATABILITY — ICE SHAPE
COLLECTED ON 2.0-IN.-DIAM CYLINDER.**

NOTES:

1. Clean Airfoil $C_d = 0.008$
2. Icing Time, 8 min for All Data
3. $P_T = 14.7$ psia for All Data
4. Collection Surface, 21 in. Chord, NACA 0012 Airfoil
5. All Data at 4-deg Angle of Attack (Ref. 3)

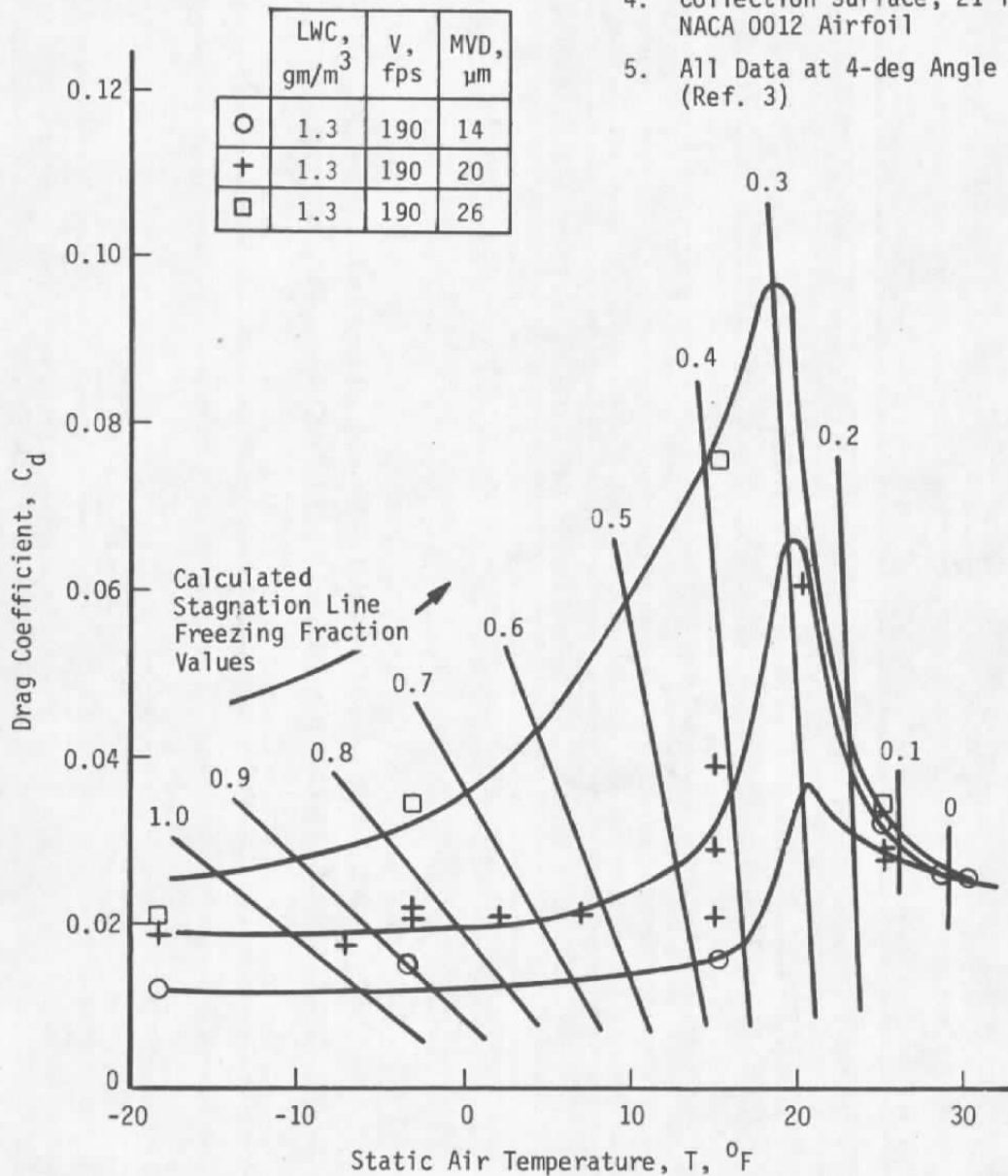


FIGURE 8. EFFECT OF STATIC AIR TEMPERATURE ON ICE SHAPE DRAG WITH LINES OF CONSTANT CALCULATED FREEZING FRACTION.

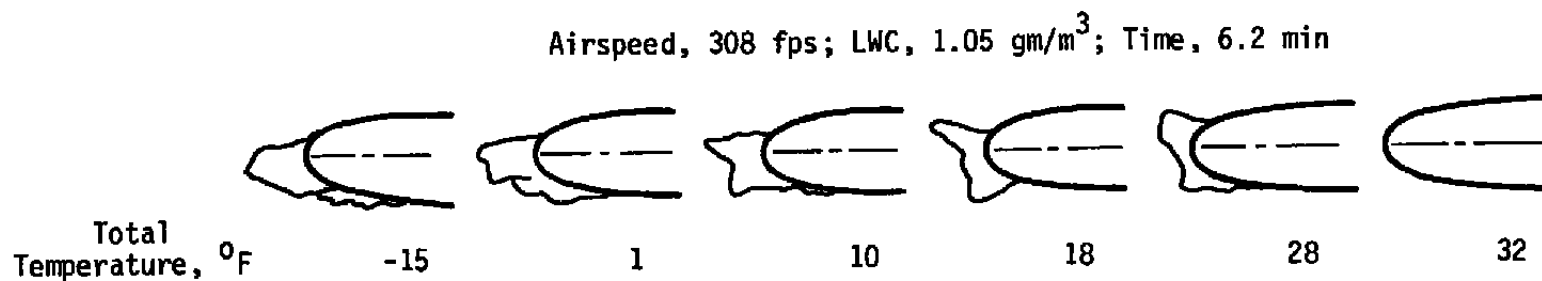
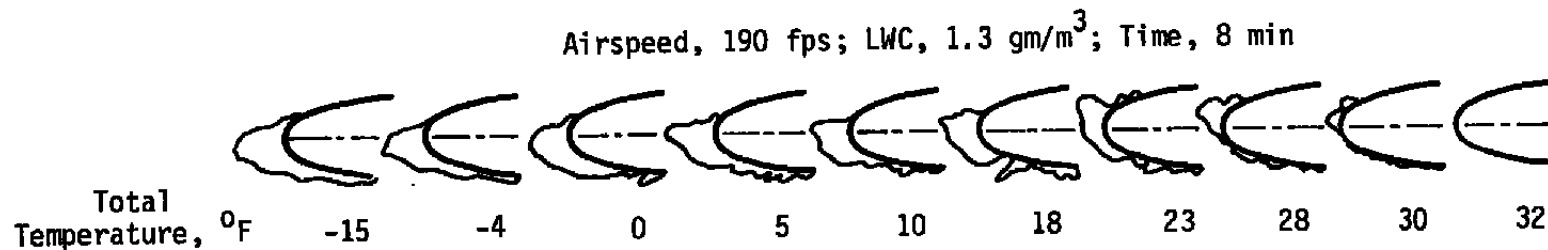


FIGURE 9. EFFECT OF TOTAL TEMPERATURE ON ICE SHAPE; $(\text{LWC} \times V \times \text{TIME}) = \text{CONSTANT}$; MVD, $20 \mu\text{M}$; AIRFOIL, NACA 0012 WITH 21-IN. CHORD AT 4-DEG ANGLE OF ATTACK (REF. 3).

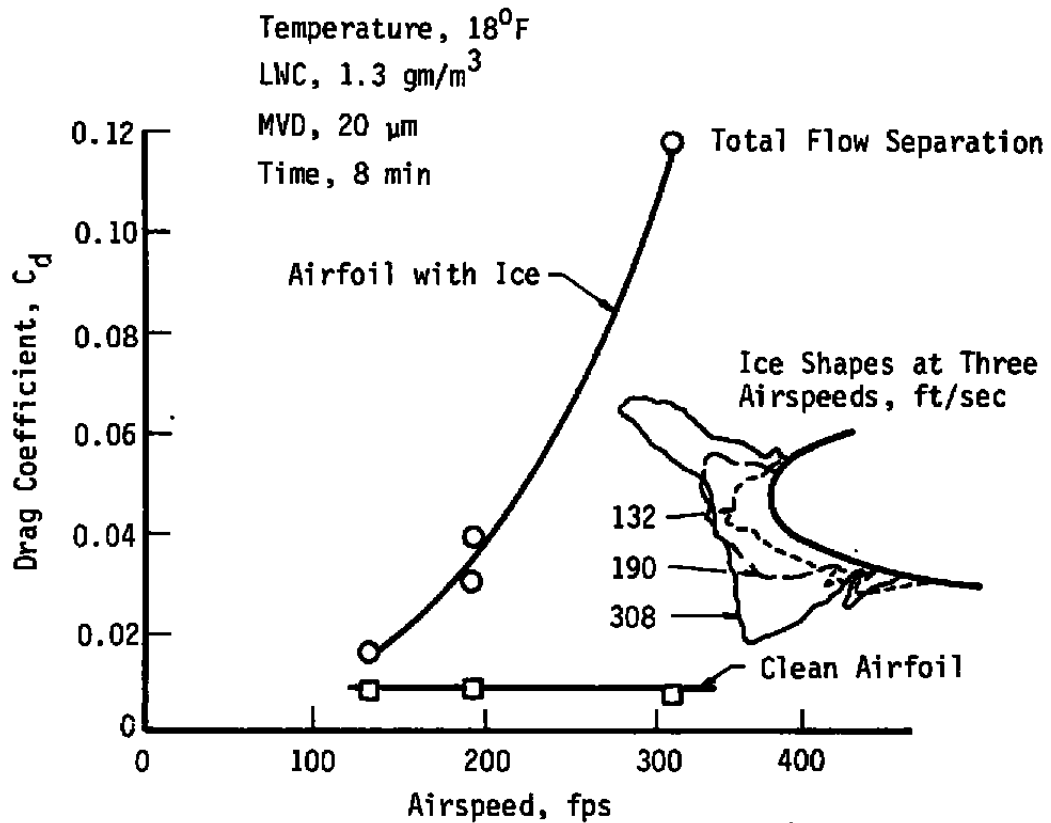
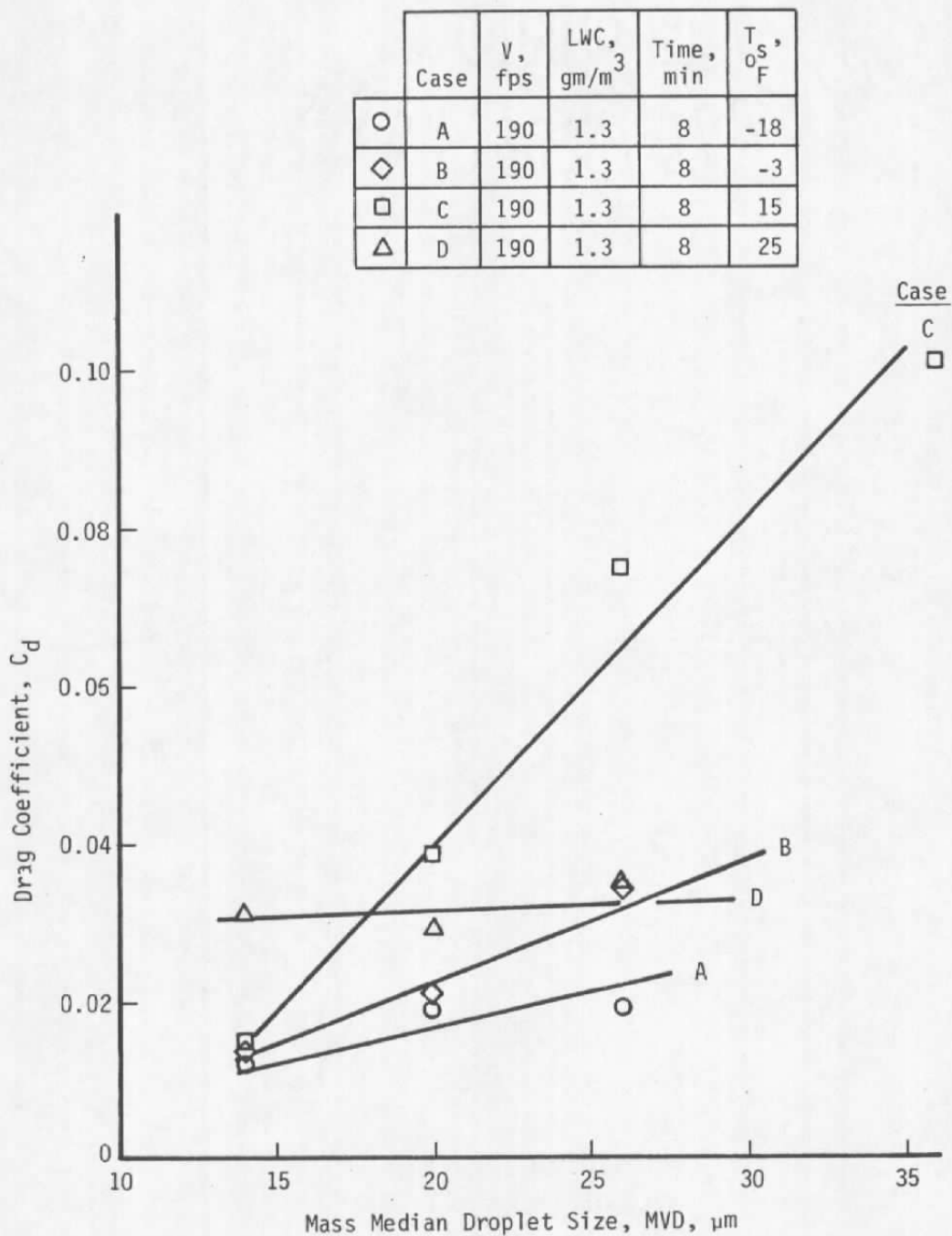
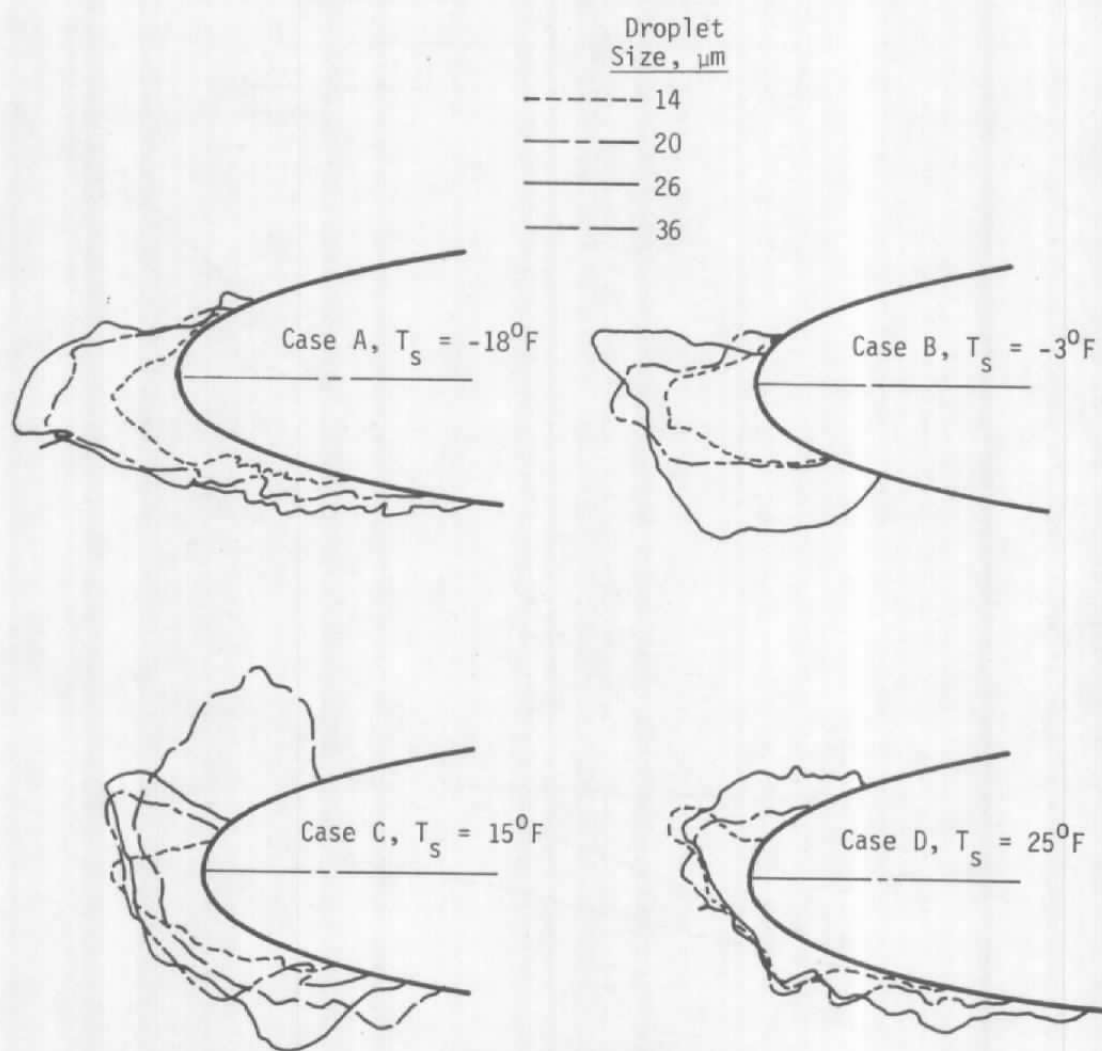


FIGURE 10. EFFECT OF VELOCITY ON ICE SHAPE AND DRAG; AIRFOIL, NACA 0012 WITH 21-IN. CHORD AT 4-DEG ANGLE OF ATTACK (REF. 3).



A. DRAG CHANGE

FIGURE 11. EFFECT OF DROPLET SIZE ON ICE SHAPE AND DRAG; AIRFOIL, NACA 0012 WITH 21-IN. CHORD AT 4-DEG ANGLE OF ATTACK (REF. 3).



B. ICE SHAPES
FIGURE 11. CONCLUDED.

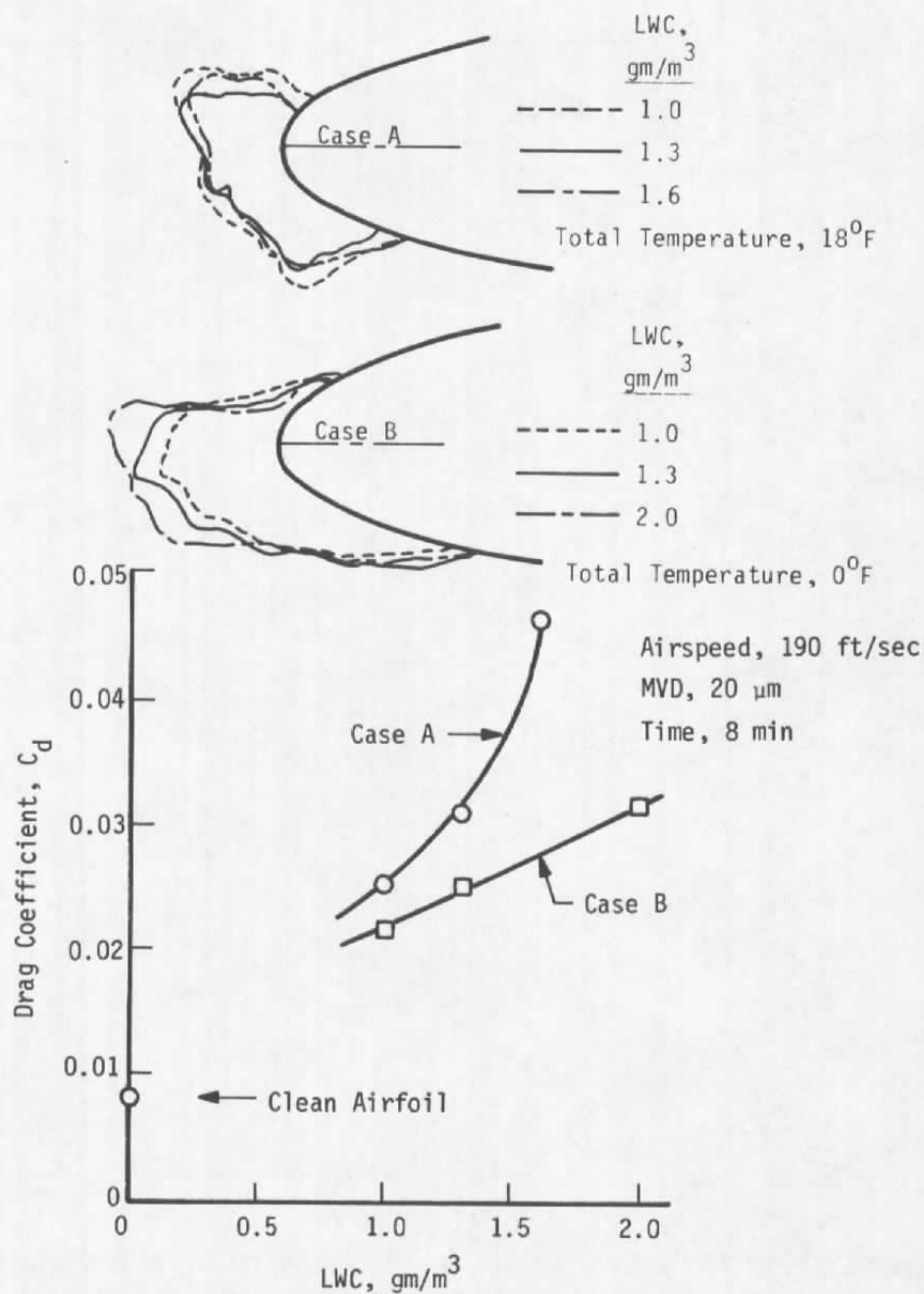
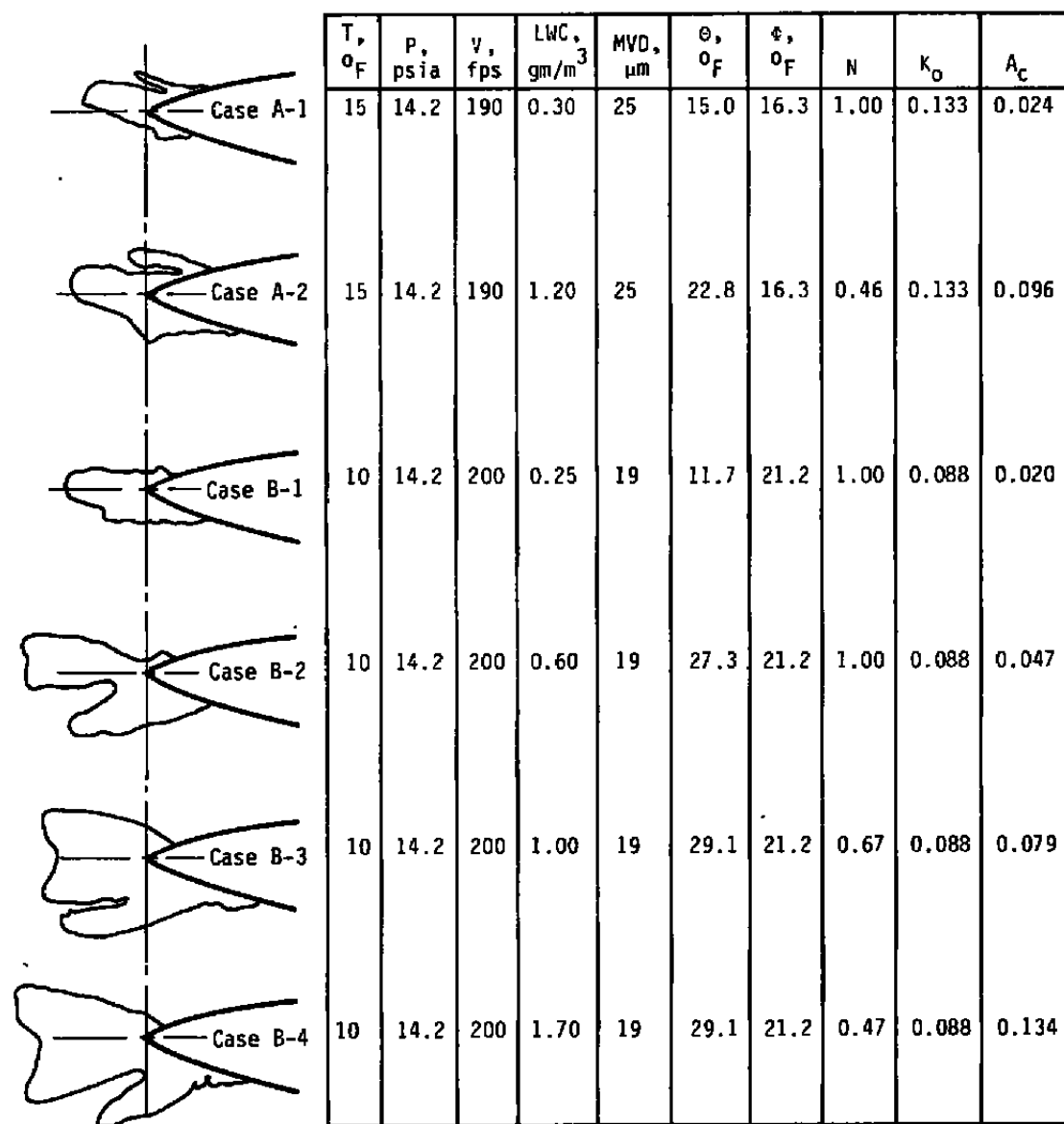
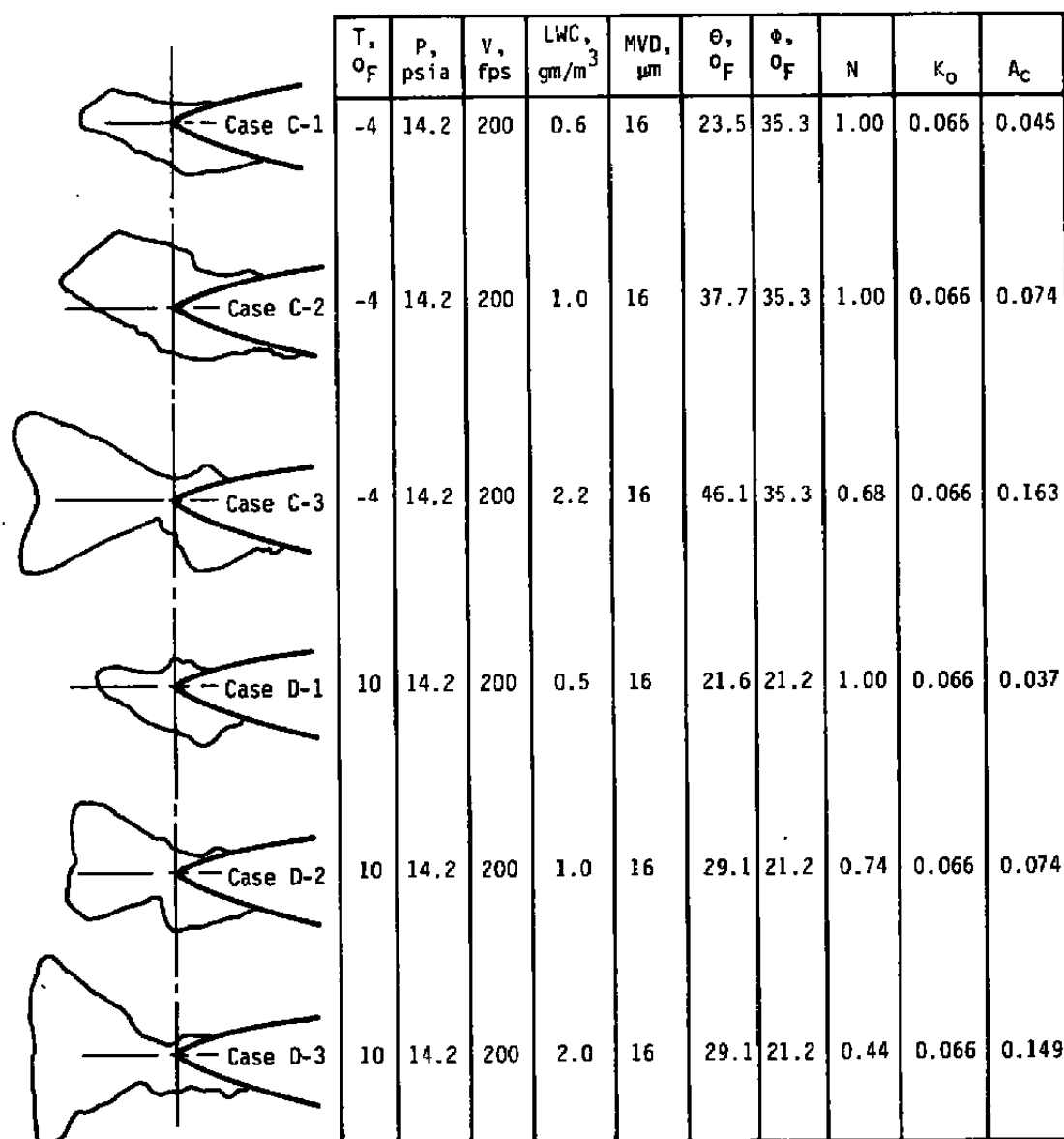


FIGURE 12. EFFECT OF LWC ON ICE SHAPE AND DRAG; AIRFOIL, NACA 0012 WITH 21-IN. CHORD at 4-DEG ANGLE OF ATTACK (REF. 3).



A. PART 1

Figure 13. EFFECTS OF LWC VARIATIONS ON LAMINAR FLOW AIRFOIL, 12-IN. CHORD, 0-DEG ANGLE OF ATTACK, 8-MIN CLOUD DURATION (SHOWN 90-PERCENT FULL-SCALE).



B. PART 2
FIGURE 13. CONCLUDED.

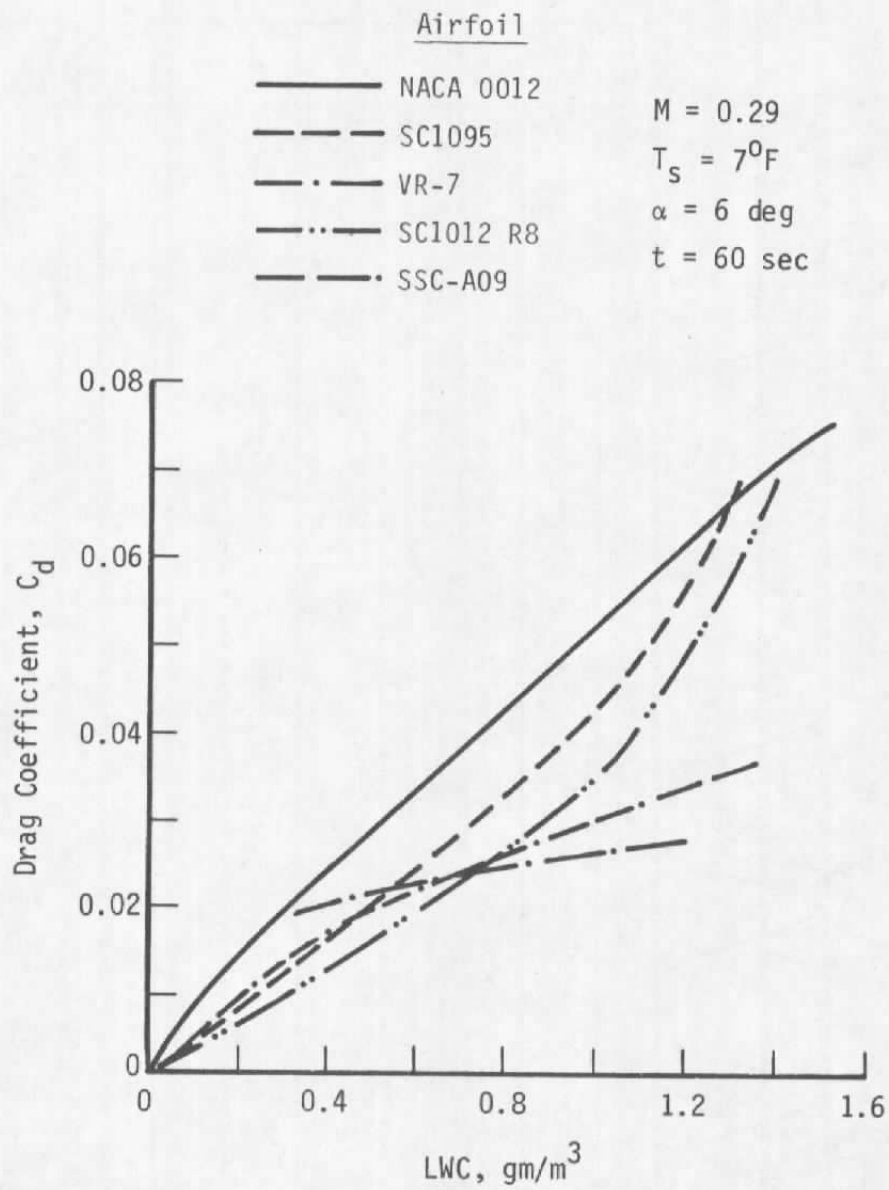
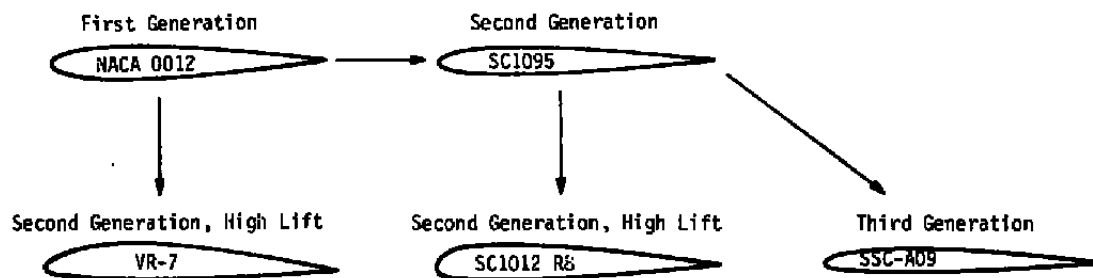


FIGURE 14. EFFECT OF LWC VARIATIONS ON DIFFERENT AIRFOILS AT THE SAME ICING TEST CONDITIONS (REF. 4).



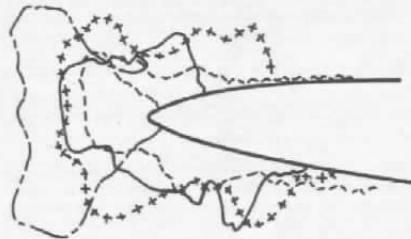
Airfoil	t/c	Chord cm (in.)	Planform Area cm ² (in. ²)
NACA 0012	0.120	15.24 (6.00)	464.5 (72.00)
SC1095	0.095	15.24 (6.00)	464.5 (72.00)
SC1012 R8	0.120	15.39 (6.00)	473.9 (73.45)
SSC-A09	0.090	15.24 (6.00)	464.5 (72.00)
VR-7	0.120	16.21 (6.38)	493.9 (76.56)

FIGURE 15. AIRFOIL GEOMETRY DETAILS (REF. 4).



$T_s, ^\circ\text{F}$	LWC, gm/m ³	MVD, μm	Time, min	V, fps	Case
-4	1.0	16	8	200	A
10	1.0	16	8	200	B
11	0.35	11	21.5	200	C

A. RIME ICE



$T_s, ^\circ\text{F}$	LWC, gm/m ³	MVD, μm	Time, min	V, fps	Case
23	2.00	30	8	200	D
28	1.90	34	8	200	E
29	0.80	13	20	200	F
28	0.80	32	20	200	G

B. GLAZE ICE

**FIGURE 16. APPROXIMATE SIMILITUDE RESULTS FOR RIME AND GLAZE ICE
BASELINE ICING CONDITIONS, LAMINAR FLOW AIRFOIL, 12-IN.
CHORD, 0-DEG ANGLE OF ATTACK.**

**TABLE 1. TABULATION OF ICING CONDITIONS AND SCALING PARAMETERS
FOR REF. 3 DATA USED IN THIS REPORT**

V, fps	T ₁ , °F	T ₂ , °F	t, min	Spray Conditions LWC, gm/m ³		C _d	β	K ₀	N	θ, °F	φ, °F
Temperature Variations											
190	-15	-18	8	1.3	20	0.019	0.669	0.053	1.00	51	49
190	-4	-7	8	1.3	20	0.018	0.670	0.053	0.92	50	38
190	0	-3	8	1.3	20	0.022	0.670	0.053	0.84	46	35
190	0	-3	8	1.3	20	0.021	0.670	0.053	0.84	46	35
190	5	2	8	1.3	20	0.021	0.670	0.053	0.71	39	29
190	10	7	8	1.3	20	0.021	0.670	0.053	0.59	33	24
190	18	15	8	1.3	20	0.029	0.670	0.053	0.41	23	17
190	18	15	8	1.3	20	0.021	0.670	0.053	0.41	23	17
190	23	20	8	1.3	20	0.060	0.670	0.053	0.28	16	11
190	28	25	8	1.3	20	0.028	0.670	0.053	0.14	8	6
190	30	27	8	1.3	20	0.026	0.670	0.053	0.09	5	4
308	-15	-23	6.2	1.05	20	0.024	0.718	0.071	1.00	53	53
308	1	6	6.2	1.05	20	0.028	0.720	0.072	0.78	44	37
308	10	3	6.2	1.05	20	0.037	0.720	0.072	0.58	34	28
308	18	10	6.2	1.05	20	0.061	0.720	0.072	0.43	25	20
308	28	21	6.2	1.05	20	0.076	0.720	0.072	0.18	10	10
Velocity Variations											
136	18	16	8	1.3	20	0.016	0.628	0.042	0.48	23	16
190	18	15	8	1.3	20	0.030	0.670	0.053	0.41	23	17
308	18	10	8	1.3	20	0.118	0.720	0.072	0.37	25	20
Drop Size Variations											
190	-15	-18	8	1.3	14	0.012	0.566	0.029	1.00	44	49
190	-15	-18	8	1.3	20	0.019	0.669	0.053	1.00	51	49
190	-15	-18	8	1.3	26	0.020	0.738	0.080	1.00	55	49
190	18	15	8	1.3	14	0.015	0.566	0.030	0.47	23	17
190	18	15	8	1.3	20	0.039	0.670	0.053	0.41	23	17
190	18	15	8	1.3	26	0.075	0.740	0.081	0.38	23	17
190	18	15	8	1.3	36	0.105	0.807	0.136	0.36	23	17
190	28	25	8	1.3	14	0.031	0.566	0.029	0.15	8	6
190	28	25	8	1.3	20	0.029	0.670	0.053	0.14	8	6
190	28	25	8	1.3	26	0.034	0.740	0.081	0.13	8	6
LWC Variations											
190	0	-3	8	1.0	20	0.021	0.670	0.053	1.00	45	35
190	0	-3	8	1.3	20	0.025	0.670	0.053	0.84	45	35
190	0	-3	8	2.0	20	0.031	0.670	0.053	0.63	45	35
190	18	15	8	1.0	20	0.026	0.670	0.053	0.50	23	17
190	18	15	8	1.3	20	0.031	0.670	0.053	0.41	23	17
190	18	15	8	1.6	20	0.046	0.670	0.053	0.36	23	17

NOTE: All Conditions at P_t = 14.7 psia

TABLE 2. SCALING PARAMETERS FOR APPROXIMATE SIMILITUDE TRIALS

Case	Test Conditions						Scaling Parameters*				
	P, psia	T, °F	LWC, gm/m ³	MVD, μm	V, fps	t, min	θ, °F	φ, °F	N ₁	K ₀	A _c
A	14.2	-4	1.0	16	200	8	37.7	35.3	1.00	0.066	0.074
B	14.2	10	1.0	16	200	8	29.1	21.1	0.74	0.066	0.074
C	14.2	11	0.35	11	200	21	13.2	20.2	1.00	0.036	0.022
D	14.2	23	2.0	30	200	8	10.9	8.2	0.15	0.184	0.178
E	14.2	28	1.9	34	200	8	3.1	3.2	0.048	0.224	0.172
F	14.2	29	0.8	13	200	20	1.4	2.2	0.054	0.047	0.055
G	14.2	28	0.8	32	200	20	3.1	3.2	0.085	0.204	0.072

* Calculated Using NACA 0012, 12-in. Chord, but 0.38-in. Leading Edge Diameter

APPENDIX A

FACILITY DESCRIPTION

Experimental icing studies are conducted in the Icing Research Test Cell (R-1D) at the AEDC (Fig. A-1). This test cell consists of a flow-metering venturi, plenum chamber, water spray system, bellmouth, removable connecting ducts, and a test chamber. Water droplets are sprayed into the primary airstream through a single, two-phase atomizing spray nozzle located in the plenum chamber, upstream of the bellmouth. The bellmouth terminates in a 12-in.-diam duct that directs the conditioned air to the test article in a 3-ft-diam test section. A secondary air system supplies air to the test section. This secondary air encapsulates the primary flow to prevent the recirculation of water droplets around the test article. The air is exhausted to the atmosphere either directly or through the Engine Test Facility (ETF) exhaust plant.

Icing studies require that both the droplet size and LWC in the test section be accurately known and controlled. The methods used for specifying these parameters are described below.

Droplet Size Calibration

A two-phase atomizing spray nozzle is used to produce a cloud of water droplets in the test cell. A cloud with the desired mass median droplet size and spray water flow rate is obtained by setting the air and water pressures supplied to the spray nozzle. Each nozzle must, therefore, be calibrated prior to use in an icing test so that the droplet size corresponding to a given set of air and water pressures is known. The droplet size distribution in the cloud is measured using a fiber-optics particle-sizing system (FOS) developed at the AEDC. The FOS is an imaging device that uses a laser beam as a light source and an optical system to define a probe volume in the droplet flow field (Fig. A-2). The probe volume is focused onto a linear array of sensor modules. As a droplet passes through the probe volume, its shadow occludes a number of the sensors. The number of sensors occluded is proportional to the droplet diameter. A thorough discussion of the operational theory of the FOS is given in Ref. A-1.

The FOS has been compared with other particle diagnostic systems including a holographic imaging system (Ref. A-2). Figure A-3 shows a comparison of the mass median diameters of droplet size distributions obtained from the FOS and the spray nozzle calibration curve obtained from holographic data. Based on this and similar comparisons, the FOS is considered to provide accurate calibrations of droplet distributions produced by water spray nozzles.

Determination of LWC

As with the droplet size measurement, the LWC is not measured on-line but is set by introducing the proper water flow into the airstream through the spray nozzle. Since the air received from the ETF air supply plant is essentially dry, considerable evaporation of the water can occur, thereby reducing the LWC. A computer code developed at the AEDC to calculate the amount of evaporation from droplets in a spray (Ref. A-3) was used to determine the additional amount of water that must be added to produce the required LWC in the test section. A comparison of methods used to determine the LWC in a test cell was done by Stallabrass (Ref. A-4) and showed that the AEDC method provided the best comparison to measured values of LWC. Calibration of the icing research test cell has been achieved by comparing the LWC predicted by the AEDC method with the LWC calculated from holographic droplet-size measurements. These results, illustrated in Fig. A-4, show that the input LWC agrees well with measured values.

Test Procedures

The spray nozzle pressures required to produce the desired water flow rate (LWC) and mass median droplet diameter were determined from the appropriate nozzle calibration curves.

After a pretest calibration of all instrumentation was performed, the test cell pressure was set to the desired pressure altitude, and primary and secondary inlet air was admitted to the test cell at the required pressure and temperature. Once the test cell flow conditions had stabilized to steady state, the desired water and air flows through the spray nozzle were set. Approximately 20 seconds were required to stabilize the cloud on a desired condition.

After exposing the test article to the icing cloud for the desired length of time, the spray nozzle and primary airflow were stopped and the test cell was brought to atmospheric pressure. The connecting duct section immediately in front of the test section (Fig. A-1) was removed and the measurements of the ice accretions were obtained. Approximately 5 minutes were required for this shutdown and measurement procedure. Since the test cell remained cold, no significant melting of the ice accretion was observed. This procedure was repeated for each test condition.

REFERENCES

- A-1. Bently, H. T. "Fiber Optics Particle-Sizing System." AEDC-TR-73-111 (AD-766647), September 1973.
- A-2. Hunt, J. D. "A Comparison of Particle Diagnostic Systems." AEDC-TR-80-33 (AD-A104027), August 1981.
- A-3. Willbanks, C. E. and Schulz, R. J. "Analytical Study of Icing Simulation for Turbine Engines in Altitude Test Cells." AEDC-TR-73-144 (AD-770069), November 1973.
- A-4. Stallabrass, J. R. "Procedure for Allowing for the Evaporation from Water Droplets in an Engine Icing Test Cell." National Research Council of Canada (NRC) Report LTR-LT-129, January 1982.

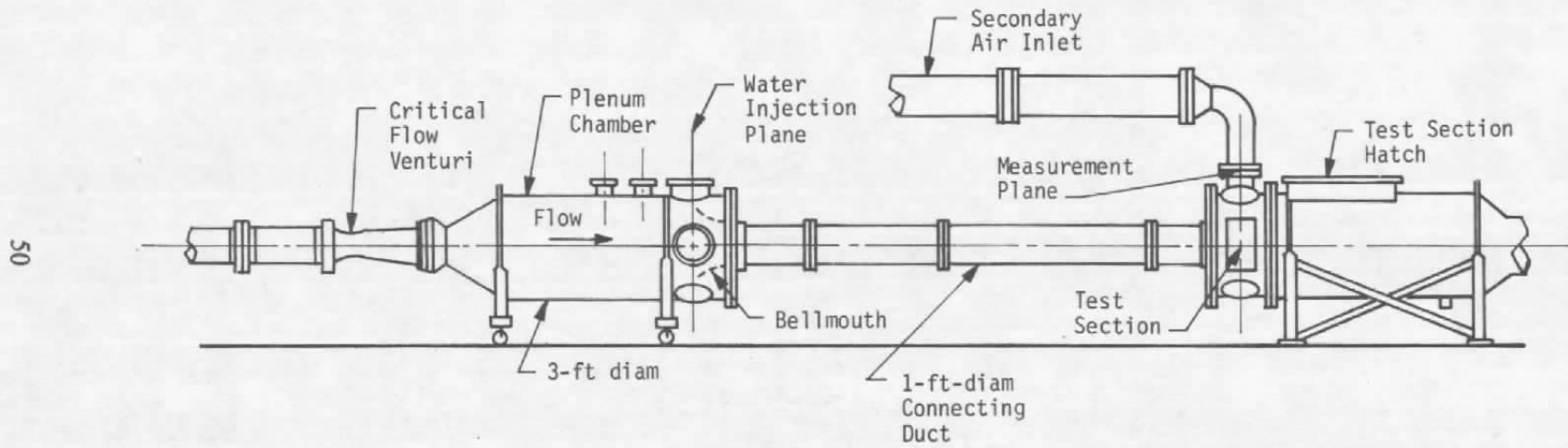


FIGURE A-1. ICING RESEARCH TEST CELL, R1-D.

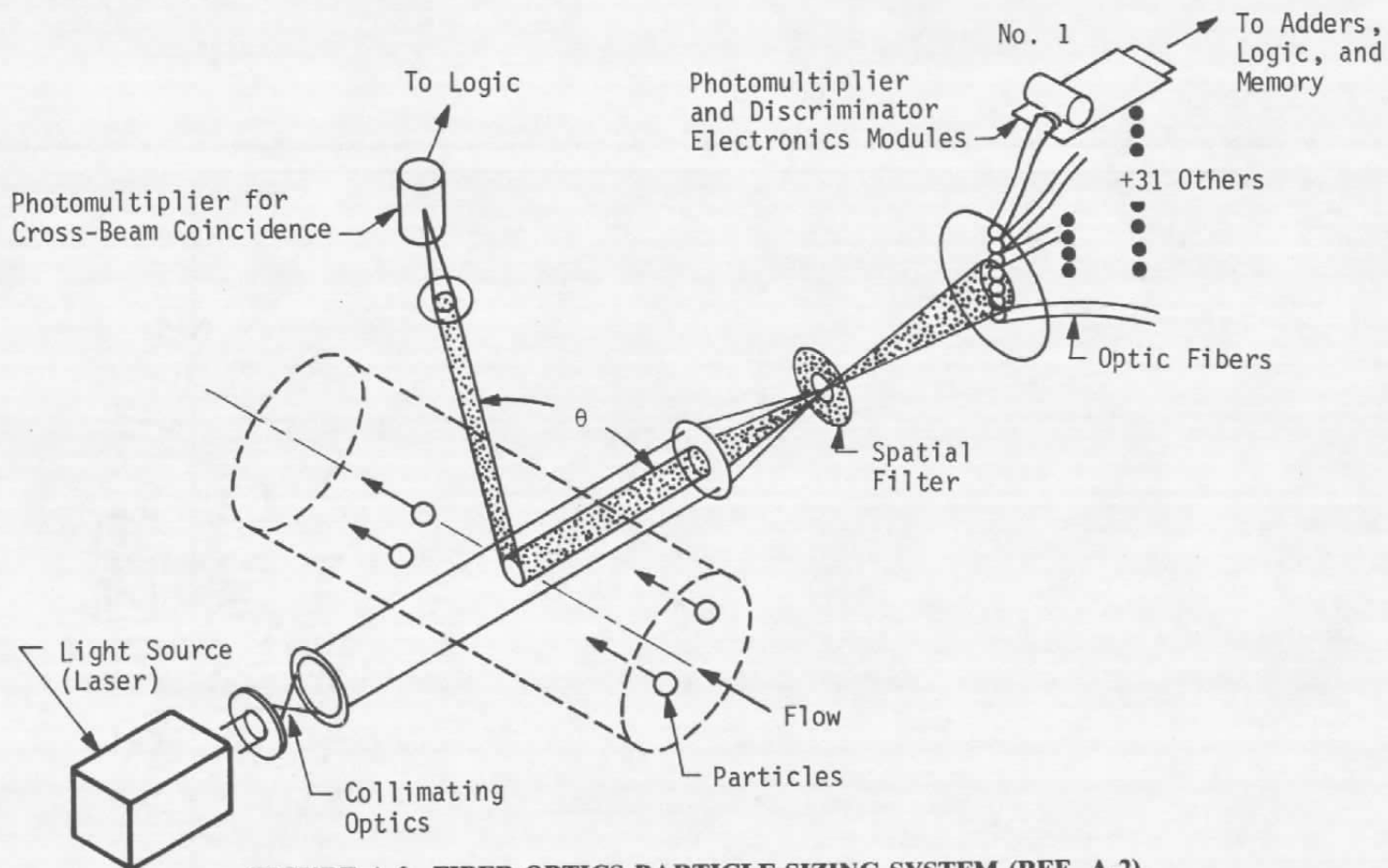


FIGURE A-2. FIBER-OPTICS PARTICLE-SIZING SYSTEM (REF. A-2).

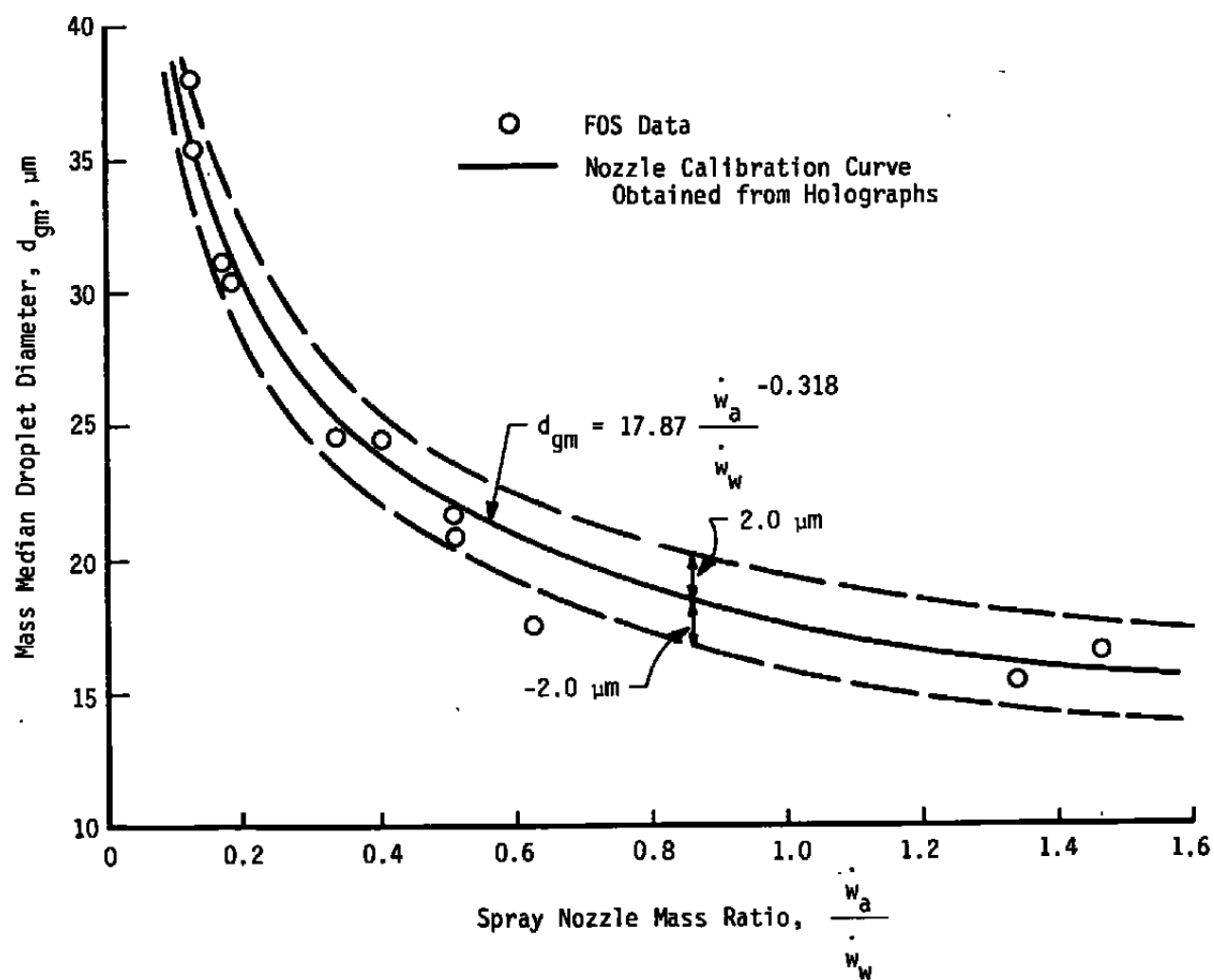
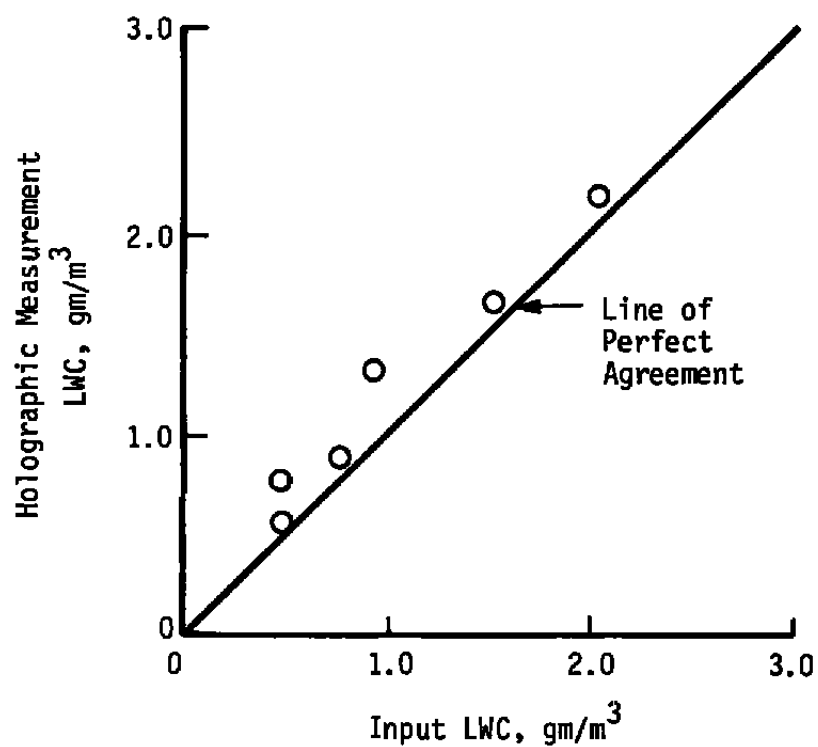


FIGURE A-3. COMPARISON OF FOS DATA WITH SPRAY NOZZLE CALIBRATION (REF. A-2).



**FIGURE A-4. COMPARISON OF INPUT AND MEASURED LWC
IN THE RESEARCH TEST CELL (REF. A-2).**

DISTRIBUTION LIST

	<u>Copies</u>		<u>Copies</u>
AEDC Technical Reports File/MS-100 Arnold AFB, TN 37389-9998	10	U.S. Air Force Flight Test Center ATTN: Kelly Adams G520 Test Group/ENAS 239 Edwards AFB, CA 93532	1
AEDC/PA Arnold AFB, TN 37389-5000	1		
AEDC/DOT ATTN: Sharon Russell Arnold AFB, TN 37389-5000	1	USAF/Aeronautical Systems Division ATTN: Steve Johnson ASD-WE Wright-Patterson AFB, OH 45433-6503	1
AEDC/DOP Arnold AFB, TN 37389-5000	1	Sverdrup Technology, Inc. ATTN: Tom Miller Box 30650 Middleberg Heights, OH 44130-9998	1
AEDC/DOPT Arnold AFB, TN 37389-5000	2		
AUL (SE)-63-508 Maxwell AFB, AL 36112	1	Continuum Dynamics, Inc. ATTN: Dr. Alan Bilanin P.O. Box 3073 Princeton, NJ 08543	5
DTIC Cameron Station Alexandria, VA 22304-6145	12	Sverdrup Technology, Inc., NSTL ATTN: Dr. J. D. Hunt, T-327 NSTL, MS 39529	1
NASA Scientific and Technical Information Facility P.O. Box 8757 Baltimore/Washington International Airport, MD 21240	3	McAir Propulsion Systems ATTN: A. M. Espinosa, MS 425 St. Louis, MO 63136	1
Hercules, Inc. Bacchus Works ATTN: H-2-100-Library P.O. Box 98 Magna, UT 84044	1	General Electric Co. ATTN: Dick Keller Aircraft Engine Group Cincinnati, OH 45215	1
Thiokol Corp. Wastach Division ATTN: Tech Library P.O. Box 524 Brigham City, UT 84302	1	Boeing-Vertol Co. ATTN: Andy Peterson, MS 32-16 P.O. Box 16858 Philadelphia, PA 19142	1
Boeing Commercial Airplane Co. ATTN: Derek Rouse, MS GL-65 P.O. Box 3707 Seattle, WA 98124-2207	1	Naval Air Test Center ATTN: Brion Picard Flight Systems Dept. Patuxent River, MD 20670	1
		University of Michigan ATTN: Gary Ruff Dept. of Aerospace Ann Arbor, MI 48104	1

	<u>Copies</u>		<u>Copies</u>
Boeing Commercial Airplane Co. ATTN: Walt Bauermeister, MS 9W-60 P.O. Box 3707 Seattle, WA 98124	1	FAA, Chief, Civil Aviation Assistance Group Madrid, Spain c/o American Embassy APO-New York 09285-0001	1
Sverdrup Technology, Inc. ATTN: Mike Barton 16530 Commerce Court P.O. Box 30650 Midpark Branch Middleburg Heights, OH 44130	1	Dick Tobiason ATA of America 1709 New York Avenue, NW Washington, DC 20006	1
Civil Aviation Authority Aviation House 129 Kingsway London WC2B 6NN England	5	FAA Anchorage ACO 701 C Street, Box 14 Anchorage, AK 99513	1
Embassy of Australia Civil Air Attache 1601 Mass. Ave., NW Washington, DC 20036	1	FAA Atlanta ACO 1075 Inner Loop Road College Park, GA 30337	1
Scientific & Tech. Info FAC ATTN: NASA Rep. P.O. Box 8757 BWI Airport Baltimore, MD 21240	1	FAA Boston ACO 12 New England Executive Park Burlington, MA 01803	1
Northwestern University Trisnet Repository Transportation Center Library Evanston, IL 60201	1	FAA Brussels ACO c/o American Embassy APO New York 09667	1
DOT-FAA AEO-500 American Embassy APO New York, NY 09667	1	FAA Chicago ACO 2300 E. Devon, Room 232 Des Plains, IL 60018	1
University of California Service Dept. Institute of Transportation Standard Library 412 McLaughlin Hall Berkely, CA 94720	1	FAA Denver 10455 East 25th Ave., Suite 307 Aurora, CO 98168	1
British Embassy Civil Air Attache ATS 3100 Mass Ave., NW Washington, DC 20008	1	Frank Taylor 3542 Church Road Ellicott City, MD 21043	1
Director DuCentre Exp DE LA Navigation Aerineene 941 Orly, France	1	Mr. Gale Braden (FAA) 5928 Queenston St. Springfield, VA 22152	1
		Richard E. Livingston, Jr. Director, Aerotech Operations for the IAPA Group 1805 Crystal Drive, Suite 1112 South Arlington, VA 22202	1

	<u>Copies</u>		<u>Copies</u>
Al Astorga Federal Aviation Administration (CAAG) American Embassy, Box 38 APO—New York 09285-0001	1	William T. Westfield, Manager Engine/Fuel Safety Branch, ACT-320 Federal Aviation Administration Technical Center Atlantic City International Airport, NJ 08405	2
Burton Chesterfield, DMA-603 DOT Transportation Safety Inst. 6500 South McArthur Blvd. Oklahoma City, OK 73125	1	Mr. Robert Koenig Engine and Propeller Standards Staff, ANE-110 Federal Aviation Administration 12 New England Executive Park Burlington, MA 01803	4
FAA Fort Worth ACO P.O. Box 1689 Fort Worth, TX 76101	1	Mr. Paul Hawkins Propulsion Branch, ANM-140S Federal Aviation Administration 17900 Pacific Highway South C-68966 Seattle, WA 98168	4
FAA Long Beach ACO 4344 Donald Douglas Drive Long Beach, CA 90808	1	Mr. Larry Kelly Helicopter Policy and Procedures Staff, ASW-110 Federal Aviation Administration P.O. Box 1689 Fl. Worth, TX 76101	2
FAA Los Angeles ACO P.O. Box 92007, Worldway Postal Center Hawthorne, CA 90009	1	Mr. Gary Frings Flight Safety Research Branch, ACT-340 Federal Aviation Administration Technical Center Atlantic City International Airport, NJ 08405	100
FAA New York ACO 181 So. Frankline Ave., Room 202 Valley Stream, NY 11581	1	Dr. Joe Shaw NASA-Lewis Research Center 21000 Brookpark Road Mail Stop 86-7 Cleveland, OH 44126	2
FAA Seattle ACO 17900 Pacific Highway South, C-68966 Seattle, WA 98168	1	Mr. Richard Adams National Resource Specialist, AWS-104 Federal Aviation Administration 800 Independence Avenue, S. W. Washington, DC 20591	2
FAA Wichita ACO Midcontinent Airport, Room 100 FAA Bldg. 1891 Airport Road Wichita, KA 67209	1		
Dr. Hans A. Krakauer Deputy Chairman, International Airline Pilots Association Group Apartado 97 8200 Albufeira, Portugal	1		
Geoffrey Lipman Executive Director, President du Conseil International Foundation of Airline Passenger Associations Case Postale 462, 1215 Geneve 15 Aeroport, Suisse, Geneva	1		

	<u>Copies</u>
Mr. Douglas E. Cosby Boeing Commercial Airplane Company P.O. Box 3707 Seattle, WA 98124	1
Dr. John Hansman Massachusetts Institute of Technology Department of Aeronautics Cambridge, MA 02139	2
Mr. Byron Phillips National Center for Atmospheric Research Research Aviation Facility P.O. Box 3000 Boulder, CO 80307	1
Mr. D. Nelepovitz Rohr Industries, Incorporated P.O. Box 878 Chula Vista, CA 92012-0878	1
Mr. Bill Gaitskill U.S. Army Aviation Systems Command 4300 Goodfellow Boulevard AMSAV-ED St. Louis, MO 63120	1
Dr. Kenneth Korkin Texas A&M University Department of Aeronautical Engineering College Station, TX 77840	1
Naval Air Propulsion Center P.O. Box 7176 Trenton, NJ 08628	1
AEDC Sverdrup Technology, Inc. C. Scott Bartlett/MS-900 Arnold AFB, TN, 37389	5

FAA INTERNAL DISTRIBUTION

ANE-40	AVS-1-Associate Administrator for Aviation Standards
ASO-52C4	
APM-13 Nigro	AWS-1-Office of Airworthiness
AEA-61	AWS-1-Aircraft Engineering Division
ADL-32 North	
AES-3	
ANM-60	
ACT-61A	
AAL-400	
M-493.2 Bldg. 10A	
APM-1	
APA-300	
AGL-60	
ASW-53B	
AAC-64D	
ACE-66	
ADL-1	
ALG-300	
ACT-5	
ASF-1-Office of Aviation Safety	
AST-1-Office of Science & Advanced Technology	
APM-1-Program Engineer & Maintenance Service	